applied sciences

MDPI

Article

Analytical Evaluation of MCE Collapse Performance of Seismically Base Isolated Buildings Located at Low-to-Moderate Seismicity Regions

Hyung-Joon Kim and Dong-Hyeon Shin *

Department of Architectural Engineering, University of Seoul, Seoul 20504, Korea; hyungjoonkim@uos.ac.kr
* Correspondence: donghyeon_shin@uos.ac.kr; Tel.: +82-02-6490-5415

Received: 6 December 2020; Accepted: 17 December 2020; Published: 21 December 2020

Abstract: The promising seismic response emerged by the concept of base isolation leads to increasing practical applications into buildings located at low-to-moderate seismicity regions. However, it is questionable that their collapse capacities can be ensured with reasonable reliability, although they would be designed according to a current seismic design code. This paper aims to investigate the collapse capacities of isolated buildings governed by the prescribed design criteria on the displacement and strength capacities of the employed isolation systems. In order to evaluate their collapse capacity under maximum considered earthquakes (MCEs), simplified numerical models are constructed for a larger number of nonlinear incremental dynamic analyses. The influential factors on the collapse probabilities of the prototype buildings are found out to specifically suggest the potential modifications of the design requirements. Although the MCE collapse probabilities of all isolated buildings are smaller than those expected for typical non-isolated buildings, these values are significantly different according to the degree of seismicity. The MCE collapse probabilities are dependent upon the governing collapse mechanism and the total system uncertainty. For the prototype buildings located at low-to-moderate seismicity regions, this study proposed the acceptable uncertainty to achieve a similar collapse performance to the corresponding buildings built at high seismicity regions.

Keywords: collapse probability; low seismicity regions; seismically isolated buildings; incremental dynamic analysis; uncertainties

1. Introduction

Base isolation has been known as one of the most effective seismic protection systems of which the desirable decoupling mechanism resulting from significant low lateral stiffness of isolators minimizes the seismic damage to superstructures [1,2]. To recognize the advantages of the base isolation system in reducing the earthquake-induced forces to a structure, its practical applications are getting popular in many construction fields [3]. Various researches have been carried out to find out the dynamic characteristics of isolated buildings incorporating various types of isolation systems [4,5] and the effects of isolation system properties on their seismic performances [6–10]. However, most of the existing research studies are focused on isolated buildings located at high seismicity regions. There is little information on the seismic performance and related design requirements of isolated buildings at low-to-moderate seismicity regions, although base isolation has been increasingly found in those regions [11], especially for buildings of which damage on contents or structural members should be strictly limited [12,13].

Based on the previous research works and the design practices, seismic design codes prescribe general design requirements for providing promising decoupling mechanisms on a superstructure and restricting excessive deformations of its isolation systems [14,15]. Current seismic design codes require

that the isolation system should be designed to accommodate the displacement demands subjected to even the maximum considered earthquake (MCE) where they should be calculated by reflecting the property uncertainties of isolation systems. Regarding this, the property modification factors are utilized to determine the upper and lower bounds of properties of isolation systems, and both the boundary properties are used to calculate the seismic responses of isolated buildings. Although the lower lateral stiffness of an isolation system might be beneficial to increase decoupling effects on the superstructure, it should satisfy the lateral restoring force requirements and in turn possess a higher post-yield stiffness ratio to limit potential residual deformations after earthquake attacks. This study is motivated by the review of the current design requirements that could induce isolation systems under large lateral displacements designed to develop the larger post-yield stiffness, even if the desirable decoupling effects are lost. This is particularly true for isolation systems equipped into buildings built at low-to-moderate seismicity regions, since they are subjected to smaller imposed lateral displacements [13]. Therefore, such design requirements for restoring the mechanism of isolation systems in a structure built at low-to-moderate seismicity regions need to be revised with ensuring the excellent seismic performance of the superstructure and limiting excessive displacements and residual deformations of the isolators.

The displacement and strength capacities of isolation systems governed by their design requirements can be sufficient to obtain the required seismic performance of isolated structures and to restrain the total system uncertainty expected for the designed isolated structures. Many sources of uncertainty contribute to variability in seismic capacity, and therefore, larger variability in the overall seismic design or evaluation procedures will necessitate larger performance levels of structures in order to control the seismic responses to an acceptable limit. For this reason, the possible uncertainty on seismic performance of isolated buildings plays an important role to determine the design requirements of isolation systems. The design requirements for isolation systems should be determined by reflecting the relation between the seismic performance of isolated buildings and the required level of total system uncertainty induced by the designed isolation systems.

The design of isolated buildings according to the current seismic codes implicitly ensures the minimum level of safety by preventing the collapse of buildings. This could be achieved by requiring an acceptably low collapse probability of structures subjected to MCE ground motions, which is based on the evaluation of their collapse capacities. In parallel with this, FEMA P695 allows a more practical assessment methodology of the performance of structures [16,17]. FEMA P695 established a consistent method for evaluating structures to ensure minimal structural safety to resist collapse and for calculating a collapse margin ratio (CMR) that can be utilized as a simple and intuitive indicator [17]. In this methodology, the CMR is computed as a ratio of the median collapse intensity to the representative intensity of an ensemble of MCE ground motion records. Using the FEMA P695 procedure, the seismic fragilities of isolated buildings were evaluated using an incremental dynamic analysis method [18]. Nakazawa et al. [19] investigated the effects of limiting the displacement demands of isolators by the use of moat walls with various clearances and behavior. Although several studies demonstrated that seismically isolated buildings have better performance than comparable typical non-isolated buildings [20–22], recent research studies focused on more rigorous evaluation of the seismic performance of isolated buildings designed according to the requirements prescribed in design codes. McVitty and Constantinou [23] investigated the reliability of the ASCE/SEI (American Society of Civil Engineers/Structural Engineering Institute) provisions using the archetypical 6-story perimeter frame isolated buildings that were assumed to be located at California, U.S., and similar analytical research works were also carried out by Kitayama and Constantinou [24].

Nevertheless, related research studies on the collapse capacities of isolated buildings are still limited and only focused on the design requirements regarding seismic effects on them. In addition, it is questionable that an acceptably low probability of collapse can be achieved for isolated buildings at low-to-moderate seismicity regions even if they are designed by current seismic codes. Therefore, this paper aims to investigate the collapse capacities of isolated buildings built

at low-to-moderate seismicity regions. The collapse capacity is mainly governed by system-level uncertainty, which is mainly influenced by the displacement and strength capacities of isolation systems determined by the prescribed design criteria. In order to clarify the relation between the collapse capacity of isolated structures and their possible uncertainty induced by design conditions, the study first starts with the design of prototype isolated buildings at both high and low-to-moderate seismicity regions. The prototype isolated buildings were designed to meet the requirements prescribed in the ASCE/SEI 7 [14]. Then, simplified numerical models were constructed for a larger number of nonlinear incremental dynamic analyses. The analysis results are presented in terms of their collapse capacities including possible uncertainties related to seismic demand and analytical modeling, and consequently, they are discussed to obtain rational collapse probabilities of such isolated buildings at low-to-moderate seismicity regions in comparison to isolated buildings at high seismicity regions of which seismic performance has been already guaranteed by many researchers. The important influential factors on the collapse probabilities of isolated buildings at low-to-moderate seismicity regions are identified, and recommendations are suggested to ensure their reliable target collapse capacity.

2. Description of Prototype Seismically Isolated Buildings

2.1. Main Design Requirements for Isolation Systems

The introduction of isolating systems into a building limits the inelastic behavior of structural members and in turn reduces potential seismic damage. This can be achieved throughout the lateral seismic displacement demands of a building being concentrated on isolators that are capable of developing significant large lateral displacement capacities without permanent damage. To assure this, a current seismic code prescribes several design requirements for isolation systems. In general, acceptable isolation systems shall (1) remain stable for required design displacements, (2) provide increasing resistance with increasing displacements, (3) not degrade under repeated cyclic loads, and (4) have quantified engineering parameters [14]. Thus, the design of isolation systems should be mainly confirmed by the codified criteria on the minimum lateral restoring forces—usually controlled by the post-yield stiffness—and the property modification factor for their nominal properties that are believed to be strongly related to the robust hysteretic behavior, as shown in Figure 1.

The current seismic code requires that bounding analyses for the property modification factor, λ of an isolation system, be performed to determine design forces variations resulting from minimum and maximum values of both effective stiffness values and energy dissipation. The property modification factor of a prototype isolation bearing is obtained from a series of characterization tests that are planned to reflect the natural variability in its properties, the effects of temperature rise during cyclic motions, and the influence of aging, contamination, and loading history. Figure 1a is a graphic presentation depicting the upper and lower bounds of the yield (or friction level) and the second slope in the lateral–force displacement relation of an isolation system. The bound values are calculated by multiplying λ factors to nominal properties. Then, the effective stiffness and damping of the isolation system are determined as both the upper and lower bound properties at the MCE displacement on the monotonic force–displacement curve.

With property variations, seismic design codes [14,15] strictly regulate lateral restoring forces that should be developed in an isolation system to limit residual and excessive displacements and consequently to ensure the acceptable safety margin in the event of after-shock or future earthquakes. As presented in Figure 1b where D_M is the total design displacement and W is the seismic weight, the isolation system shall be configured, for both upper and lower bounds of isolation system properties, to produce the lateral restoring force such that the lateral force at the corresponding maximum displacement is at least $0.025W$ of the superstructure greater than the lateral force at 50% of the corresponding D_M.

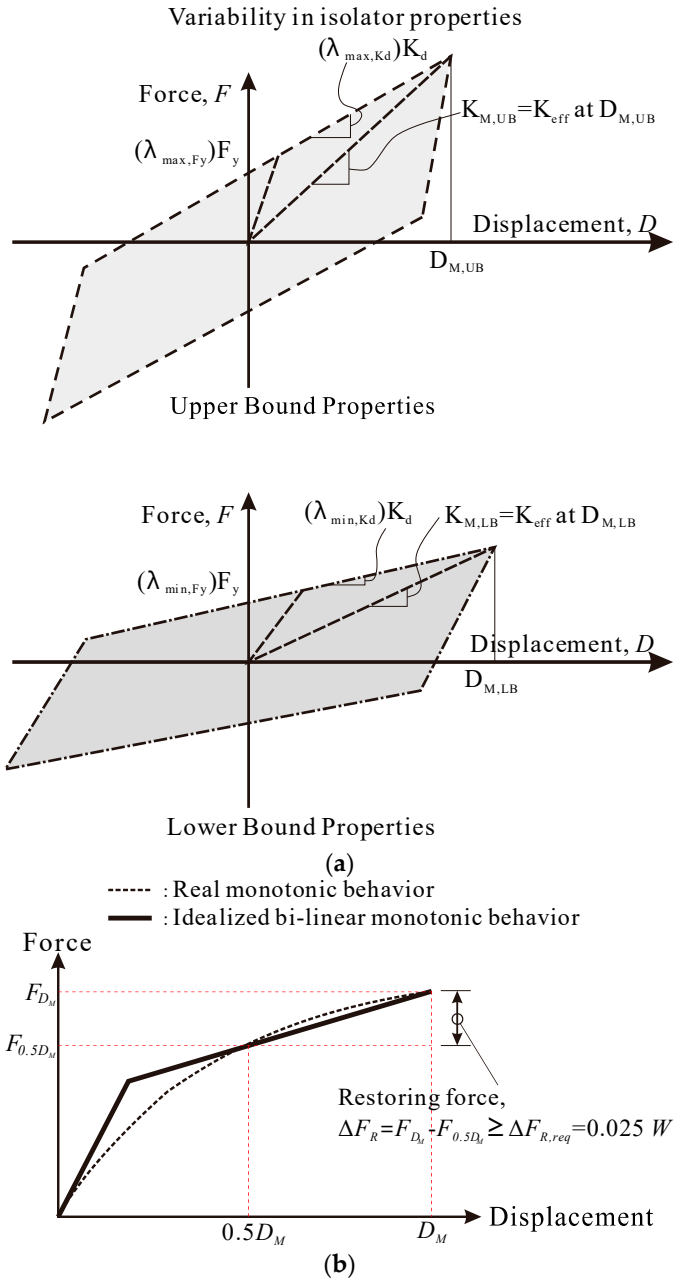

Figure 1. Main design requirements for isolation systems (ASCE, 2016): (**a**) Property modification factors; (**b**) Lateral restoring force.

The monotonic force–displacement behavior of an isolation system is characterized with the three parameters of the yield strength, Q_y, the yield displacement, D_y, and the post-yield stiffness, k_d. Of them, the first two parameters are closely related to the design wind load condition. The lower bound value of Q_y is usually determined to be equal to or greater than the design wind loads imposed to the building. The value of D_y would be determined by the requirement that the lateral displacements in an isolating story shall not be larger than those between floors in the superstructure when subjected to wind loads. These two requirements enable the isolation systems to avoid wind-induced permanent plastic deformations. The last parameter, k_d is strongly related to the criterion on lateral restoring forces which the isolation system has to be capable of developing. The isolation system with low effective stiffness can easily attain the criterion on lateral restoring forces, $\Delta F_{R,req}$, if it expects to be subjected to a large value of D_M. This is especially relevant for isolation systems employed into a building at high

seismicity region. However, the desirable decoupling effect of isolation systems at low-to-moderate seismicity regions could be lost, since small displacement demands at low-to-moderate seismicity regions induces relatively large effective stiffness in order to obtain the required lateral restoring force $\Delta F_{R,req}$. For such isolation systems, the further loss of decoupling effects might lead from the introduction of the values of k_d multiplied with a λ factor.

2.2. Design of Seismically Isolated Buildings

The framing plane of three, five, and ten-story isolated buildings previously studied by Shin and Kim [13] were selected as the prototype buildings. Figure 2 presents the configuration of buildings of which the plan is 21 m by 21 m with a story height of 3.5 m. The intermediate reinforced concrete (RC) moment-resisting frames adopted as lateral force resisting systems and isolation systems were designed according to the provisions of ASCE/SEI 7 [14]. For the maintenance and inspection of isolators and their connecting members, the isolating story-height of each prototype building was assumed to be 2500 mm. In order to compare the collapse probabilities of isolated buildings located at low-to-moderate seismicity regions to those of corresponding buildings at high seismicity regions, the prototype buildings were designed according to different levels of seismic hazards. As shown in Table 1a, different wind load conditions were considered in designing prototype buildings in order to reflect the contribution of the design wind load as well as the design seismic load on determining the force–displacement relation of an isolation system. For the seismic design of a series of prototype buildings, some of them were assumed to be built at high seismicity regions of which the MCE spectral accelerations at short and 1-s periods are S_S = 1.50 g and S_1 = 0.60 g, respectively. The spectral accelerations, S_S = 0.46 g and S_1 = 0.19 g, were selected as the representative of moderate seismicity and applied for the seismic design of the other prototype buildings. The isolated buildings were located on a soil condition with site class C (with shear wave velocity V_{S30} = 360 to 760 m/s). Using the seismic design parameters summarized in Table 1b, the preliminary design according to the equivalent lateral force method had been carried out to confirm the minimum design criteria and to calculate member forces. Then, a dynamic analysis procedure was utilized to validate the design results of the prototype isolated buildings. A more detailed design procedure of the prototype isolated buildings can be found in the research of Shin and Kim [13].

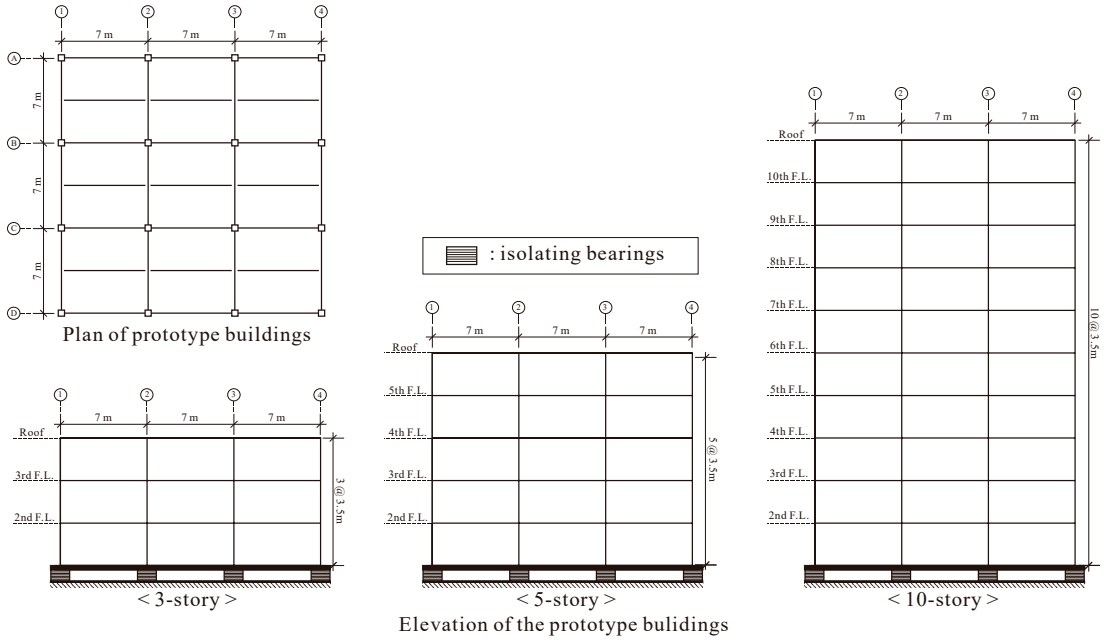

Figure 2. Building plan and elevation of prototype isolated buildings.

Table 1. Design parameters of prototype isolated buildings.

(a) Wind Load Conditions					
-		**Exposure Category**		**Basic Wind Speed, m/s**	
Strong windy load		C		30	
Weak windy load		B		40	
(b) Seismic Design Parameters					
R	Ω_0	C_d	I	R_I	**Site Class**
5	3	4.5	1.0	1.875	C

Note: R is the response modification factor, Ω_0 is the over-strength factor, C_d is the displacement amplification factor, and I is the important factor.

Using isolators including lead rubber bearings (LRBs), natural rubber bearings (NRBs), and friction sliding bearings (FSBs) shown in Figure 3, their capacities and distributions on the isolating floor plane were determined to meet the design requirements for lateral restoring forces and property modification factors. This study utilizes experimental results described by Shin and Kim [13]. To specify realistic values for the stiffness and strength of isolators, the nonlinear force–displacement properties of LRBs and NRBs were obtained from cyclic test results shown as a black line in Figure 3. According to the method of prototype test described in ASCE/SEI 7 [14], hysteretic behaviors were evaluated. The cyclic tests were performed for three fully reversed cycles of loading at the maximum displacement. The vertical load was considered as the average dead load plus one-half the effects due to live load on isolating bearings. The NRBs remained elastic subjected to the maximum displacement and linear hysteretic behaviors were adopted for shear deformation, while the LRBs presented a yield of lead bar embedded in isolating bearings. In comparison to the acceptance criteria defined as ±15% variations for the nominal design values, test results for isolators were validated, since test results for the stiffness and strength characteristics fell within the range of acceptance criteria.

Table 2 summarizes the monotonic properties of isolators selected for the prototype buildings. Since the isolation systems should remain elastic under wind loading, their lower bound properties for Q_y values should be equal to at least the design wind load of each prototype building. A value of $\Delta F_{R,req}$ for the restoring force criterion of isolation systems is 2.5% of the seismic weight and thus, it is similar for the prototype buildings with the same number of stories. The lower bound ΔF_R values of isolation systems at the high seismicity regions resulting in the larger deformation demands are larger than those at the low seismicity regions. Figure 4 illustrates the monotonic properties of the isolation systems that were designed to satisfy the required lateral restoring forces differentiating according to design conditions. Table 3 compares the seismic design values of the prototype buildings and the mean, lower, and upper properties of the isolation system. With the increase in the $\Delta F_{R,req}$ and a number of stories of the prototype building, the required effective stiffness is increased, which results in the decrease of the fundamental effective periods, T_M. It is clearly shown from values of T_1/T_M in the table that the T_M values of all prototype isolated buildings are lengthened compared to the 1st modal periods, T_1, of the corresponding fixed structures. Note that the largest values of T_1/T_M are found in the prototype buildings designed with smallest seismic design load and largest design wind loads.

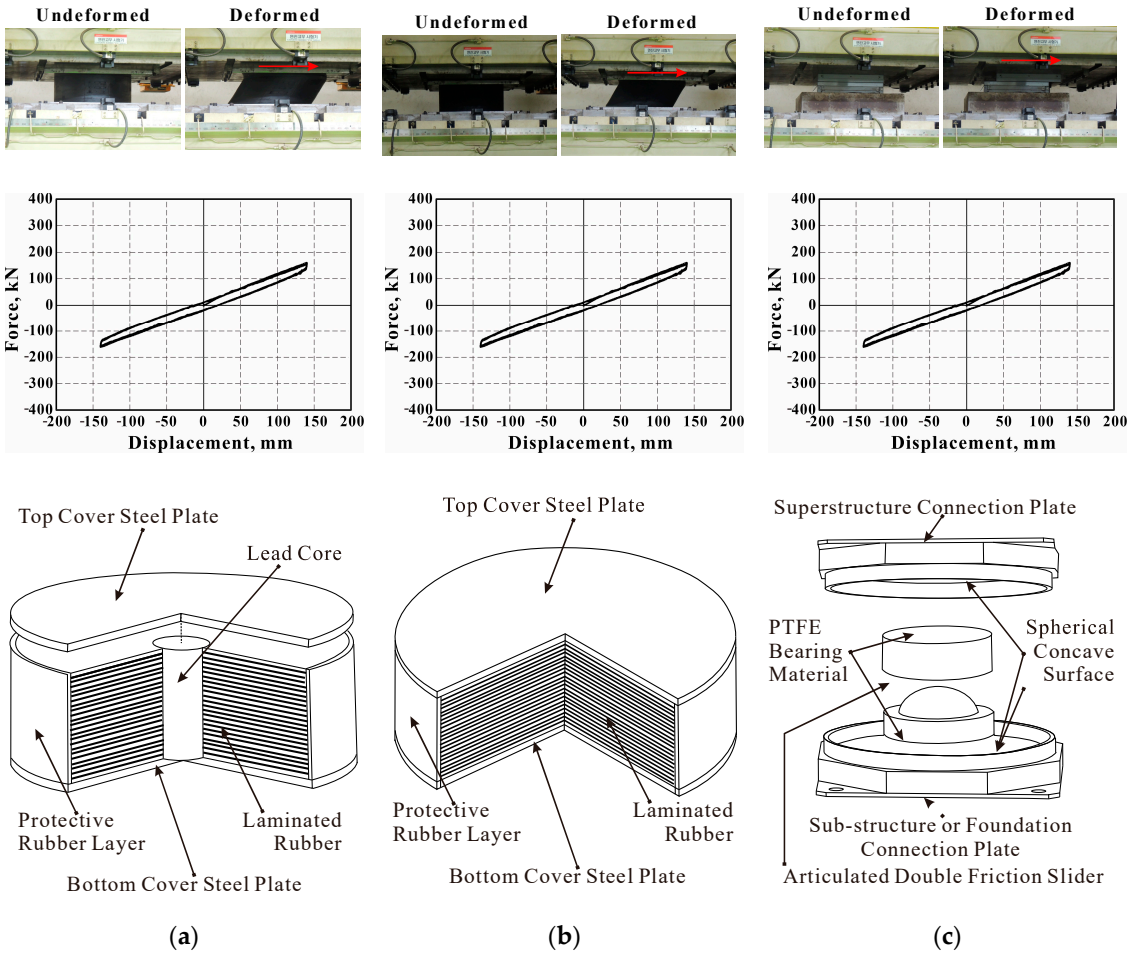

Figure 3. Configurations and experimental results of typical isolations (after Shin and Kim [13]; Christopoulus and Filiatrault [25]): (**a**) Lead rubber bearing (LRB); (**b**) Natural rubber bearing (NRB); (**c**) Friction sliding bearing (FSB).

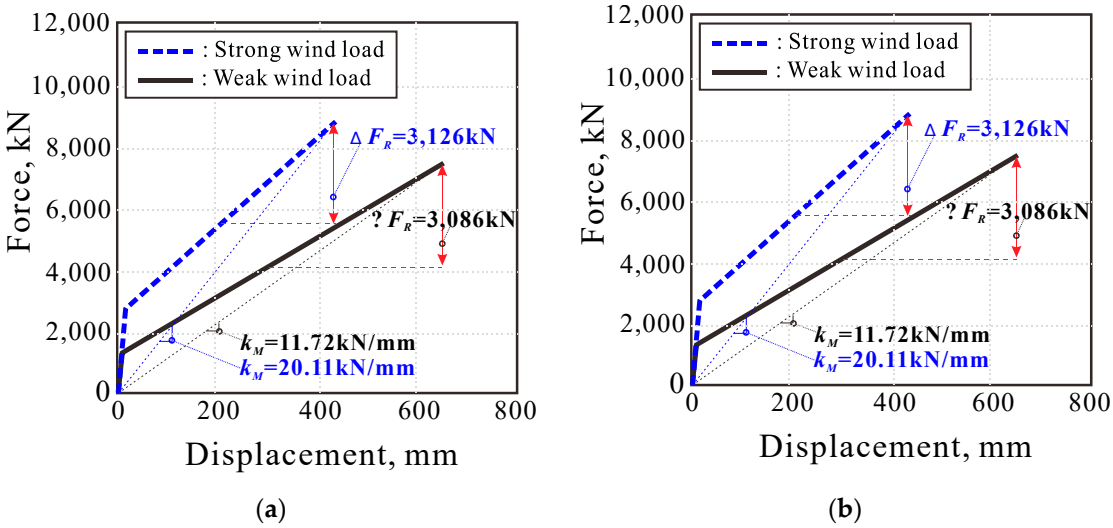

Figure 4. Comparison of force–displacement relations of isolation systems (10-story isolated buildings): (**a**) High seismicity regions; (**b**) Low-seismicity regions.

Table 2. Summary of monotonic properties of isolation systems designed with ASCE/SEI 7 [14].

(a) Building at High Seismicity Region																		
-	**Under Strong Windy Load**									**Under Weak Windy Load**								
	3-Story			**5-Story**			**10-Story**			**3-Story**			**5-Story**			**10-Story**		
	3S$_E$40C			**5S$_E$40C**			**10S$_E$40C**			**3S$_E$30B**			**5S$_E$30B**			**10S$_E$30B**		
	LB	**M**	**UB**	**LB**	**M**	**UB**	**LB**	**M**	**UB**	**LB**	**M**	**UB**	**LB**	**M**	**UB**	**LB**	**M**	**UB**
k_e	68	86	86	140	140	140	186	186	186	48	48	48	76	76	76	128	128	128
k_d	4.7	6.6	8.9	8.7	11.0	14.9	11.6	14.4	19.9	2.8	3.6	4.7	4.3	5.4	6.9	7.6	9.6	12.7
k_{eff}	5.5	8.1	11.3	10.4	13.3	18.7	15.5	20.1	29.5	3.4	4.3	6.0	5.3	6.7	9.1	9.2	11.7	16.2
Q_y	498	622	933	917	1146	1719	2177	2722	4083	298	373	559	399	499	748	1036	1295	1942
D_M	489	402	314	483	417	333	506	435	339	632	551	441	666	577	451	744	644	514
$\Delta F_{R,req}$	328	328	328	571	571	571	1271	1271	1271	328	328	328	568	568	568	1271	1271	1271
ΔF_R	1150	1948	2056	2103	2292	2476	2931	3126	3375	895	983	1041	1427	1546	1551	2837	3086	3267
(b) Building at Low-to-Moderate Seismicity Region																		
-	**Under Strong Windy Load**									**Under Weak Windy Load**								
	3-Story			**5-Story**			**10-Story**			**3-Story**			**5-Story**			**10-Story**		
	3L$_E$40C			**5L$_E$40C**			**10L$_E$40C**			**3L$_E$30B**			**5L$_E$30B**			**10L$_E$30B**		
	LB	**M**	**UB**	**LB**	**M**	**UB**	**LB**	**M**	**UB**	**LB**	**M**	**UB**	**LB**	**M**	**UB**	**LB**	**M**	**UB**
k_e	70	89	89	122	122	123	199	200	201	59	59	59	78	79	79	135	136	139
k_d	5.1	9.4	12.9	10.4	12.8	14.5	24.0	32.1	43.3	3.5	4.5	5.9	7.1	9.0	12.7	15.9	23.5	30.6
k_{eff}	9.4	15.8	24.7	18.5	24.8	39.7	37.7	50.5	81.0	5.0	6.5	9.6	8.8	11.3	16.6	20.3	24.7	38.4
Q_y	498	622	933	929	1160	1741	2177	2722	4083	241	302	453	399	499	748	1036	1295	1942
D_M	110	84	65	98	84	66	103	89	72	163	142	110	178	154	116	161	155	111
$\Delta F_{R,req}$	306	306	306	531	531	531	1152	1152	1152	306	306	306	531	531	531	1152	1152	1152
ΔF_R	420	581	615	754	790	781	1236	1432	1558	425	475	477	632	689	738	1279	1821	1692

Note: LB is the lower bound property, M is the mean property, UB is the upper bound property, k_e is the elastic stiffness (kN/mm), k_d is the 2nd stiffness (kN/mm), k_{eff} is the effective stiffness (kN/mm), Q_y, is the yield strength (kN), D_M is the maximum displacement of isolation system (mm), $\Delta F_{R,req}$ is the required lateral restoring force (kN), ΔF_R is the restoring force of isolation system (kN).

Table 3. Summary of design results of isolated buildings.

(a) Building at High Seismicity Region																		
-	**Under Strong Windy Load**									**Under Weak Windy Load**								
	3-Story			**5-Story**			**10-Story**			**3-Story**			**5-Story**			**10-Story**		
	3S$_E$40C			**5S$_E$40C**			**10S$_E$40C**			**3S$_E$30B**			**5S$_E$30B**			**10S$_E$30B**		
	LB	**M**	**UB**	**LB**	**M**	**UB**	**LB**	**M**	**UB**	**LB**	**M**	**UB**	**LB**	**M**	**UB**	**LB**	**M**	**UB**
T_1		0.49			0.69			1.12			0.49			0.69			1.12	
T_M	3.11	2.56	2.16	2.97	2.63	2.22	3.63	3.19	2.63	3.94	3.49	2.98	4.17	3.70	3.17	4.72	4.18	3.55
T_1/T_M	0.16	0.19	0.23	0.23	0.26	0.31	0.31	0.35	0.43	0.12	0.14	0.16	0.17	0.19	0.22	0.24	0.27	0.32
$\beta_{eq,M}$	11.1	11.2	14.6	9.8	10.7	13.1	16.4	17.4	20.4	10.5	11.0	13.7	10.5	11.5	14.1	11.0	12.0	14.7
B_M	1.23	1.24	1.34	1.19	1.22	1.29	1.39	1.42	1.51	1.21	1.23	1.31	1.22	1.25	1.36	1.23	1.26	1.34

Table 3. *Cont.*

(b) Building at Low-to-Moderate Seismicity Region																		
-	Under Strong Windy Load									Under Weak Windy Load								
	3-Story			5-Story			10-Story			3-Story			5-Story			10-Story		
	$3L_E40C$			$5L_E40C$			$10L_E40C$			$3L_E30B$			$5L_E30B$			$10L_E30B$		
	LB	M	UB	LB	M	UB	LB	M	UB	LB	M	UB	LB	M	UB	LB	M	UB
T_1	0.70			1.00			1.49			0.70			1.00			1.49		
T_M	2.29	1.78	1.46	2.15	1.86	1.46	2.22	1.91	1.51	3.14	2.76	2.27	3.12	2.73	2.27	3.02	2.74	2.20
T_1/T_M	0.31	0.39	0.48	0.47	0.54	0.68	0.67	0.78	0.99	0.22	0.25	0.31	0.32	0.37	0.44	0.49	0.54	0.68
$\beta_{eq,M}$	22.9	24.2	26.5	27.7	28.1	28.6	25.9	25.7	23.8	18.1	18.4	22.5	13.8	14.7	16.6	16.9	14.3	17.7
B_M	1.56	1.58	1.63	1.65	1.66	1.67	1.62	1.61	1.58	1.44	1.45	1.55	1.32	1.34	1.45	1.41	1.33	1.75

Note: LB is the lower bound property, M is the mean property, UB is the upper bound property, T_1 is the 1st modal period of superstructures (s), T_M is the effective period at the D_M (s), $\beta_{eq,M}$ is the effective damping ratio under MCE, B_M is the damping coefficient at the D_M, D_M is the maximum displacement.

3. Collapse Performance of Seismically Isolated Buildings

3.1. Analysis Models of Isolated Buildings

A detailed analysis model representing the prototype buildings had been constructed and was then simplified to a lumped-mass-and-spring model that is known to tailor for incremental dynamic analyses requiring a significantly large number of analyses. The responses and dynamic characteristics of a superstructure obtained from both the models will be compared to calibrate the simplified model, which will be discussed in detail later. There are several assumptions implemented into both the analysis models for the prototype buildings. An inherent damping ratio is assumed to be 2% of critical for all modes [24]. Nonlinear analyses are carried out with the Newmark–Beta method that has been typically used to capture nonlinear dynamic responses with reasonable analytical stability. Dynamic equilibrium is calculated every specific time step, which is less than the time-step of earthquake records selected for this study mentioned later. The iterative Newton–Raphson method used for checking the dynamic equilibrium can provide reasonable numerical results with the overshoot tolerance of 1%. A P-delta effect is explicitly considered in the analysis model, and seismic masses in each floor are considered to be lumped at its center with the typical assumption of the rigid diaphragm. This study did not explicitly consider the pounding effects of seismically isolated buildings to the moat wall under a large displacement of isolation systems [26,27].

The detailed analysis model was constructed using commercial software, PERFORM 3D [28]. Frame Member Compound components were utilized to model structural members in the superstructures and isolators of NRBs and LRBs were modeled with built-in Rubber Type Seismic Isolator elements. According to the prototype test results of isolators presented in Shin and Kim [13] showing that they are almost linear responses under maximum displacements, the NRBs were modeled with linear hysteretic elements. The idealized bi-linear behavior was implemented for the LRBs to model the yielding phenomenon of their embedded lead bars and their hyper-elastic stiffening occurring at large displacements was neglected, since their allowable deformation capacities are assumed to be sufficiently large enough, as considered in their typical designing phase. The FSBs were modeled using built-in Friction Pendulum Seismic Isolator elements with a friction coefficient of 0.0024. The restoring force of the very stiff FSB bearing elements in compression is independent of shear deformations after sliding. Each component consists of rigid end zones located at both ends, and an inelastic element representing its sectional properties between the ends. The lengths of the rigid zones are assumed to be half of the connected column width or beam depth. The deterioration behavior of the elements was modeled, and failure was implicitly accounted for by limiting on a story drift of 2%.

The simplified lumped mass model (SLMM) is utilized in the condition that each story in the superstructure above the isolation system is to be modeled with an elasto-plastic spring, and the

prototype isolated buildings with symmetric planes have no eccentricity. No overturning is also assumed to occur in the superstructure during seismic loading. As shown in Figure 5, the SLMM consists of the multi-spring assemblage located on the top of a shear spring representing the hysteretic behavior for an isolation system. The spring assemblage representing the entire superstructure consists of in-series connected transverse springs with the stiffness, $K_{s,i}$, and the yield strength, $F_{s,i}$. The structural properties of the yield strength, initial stiffness, and post-yield stiffness of the transverse spring representing the story in the superstructure are determined by the procedure as follows:

(1) With a lateral load pattern corresponding to the yield displacement of the superstructure, δ_y is then obtained. Then, the yield displacement of the ith story, d_{yi}, is calculated by multiplying the relative eigenvector $\{f_{i+1} - f_i\}$ and the value of δ_y.

(2) The stiffness of spring elements, $K_{s,i}$, is determined by introducing the coefficient for modifying the stiffness, ρ_i to the seismic weight over relative eigenvector, $W_i/\{f_{i+1} - f_i\}$. The value of ρ_i can be obtained throughout iterations by changing it until the difference between T_1 and $\{f_i\}$ of the SLMM and those of the detailed model is sufficiently small.

(3) The yield strength of spring elements, $Q_{s,i}$ is determined by multiplying $K_{s,i}$ and d_{yi}. Until the difference between the strength obtained from the SLMM and detailed model is sufficiently small, the $Q_{s,i}$ value is modified by introducing the coefficient for modifying the strength, γ_i.

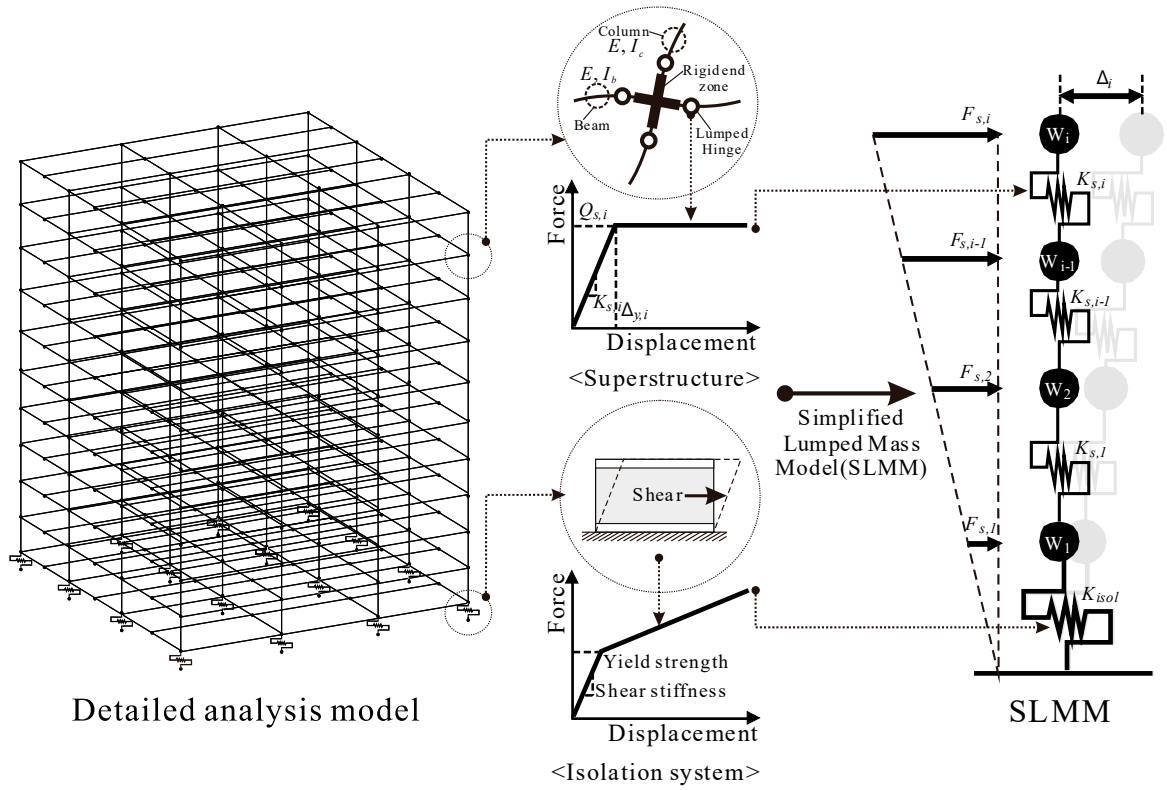

Figure 5. Description of simplified lumped mass model.

Figure 6a shows the comparison of the first mode periods and mode shape vectors obtained from the detailed model and the SLMN of the superstructure. Similarity on the base shear and story drift relations obtained from both models can be found in the figure. In addition, Figure 6b illustrates the comparison between the analysis results of the SLMM and the detailed model excited by MCE ground acceleration records. The elastic and effective periods under MCEs have a difference less than 10% for both the analysis models. In addition, the mean values of maximum floor accelerations and story displacements obtained from the SLMM are well-matched with those of the detailed model.

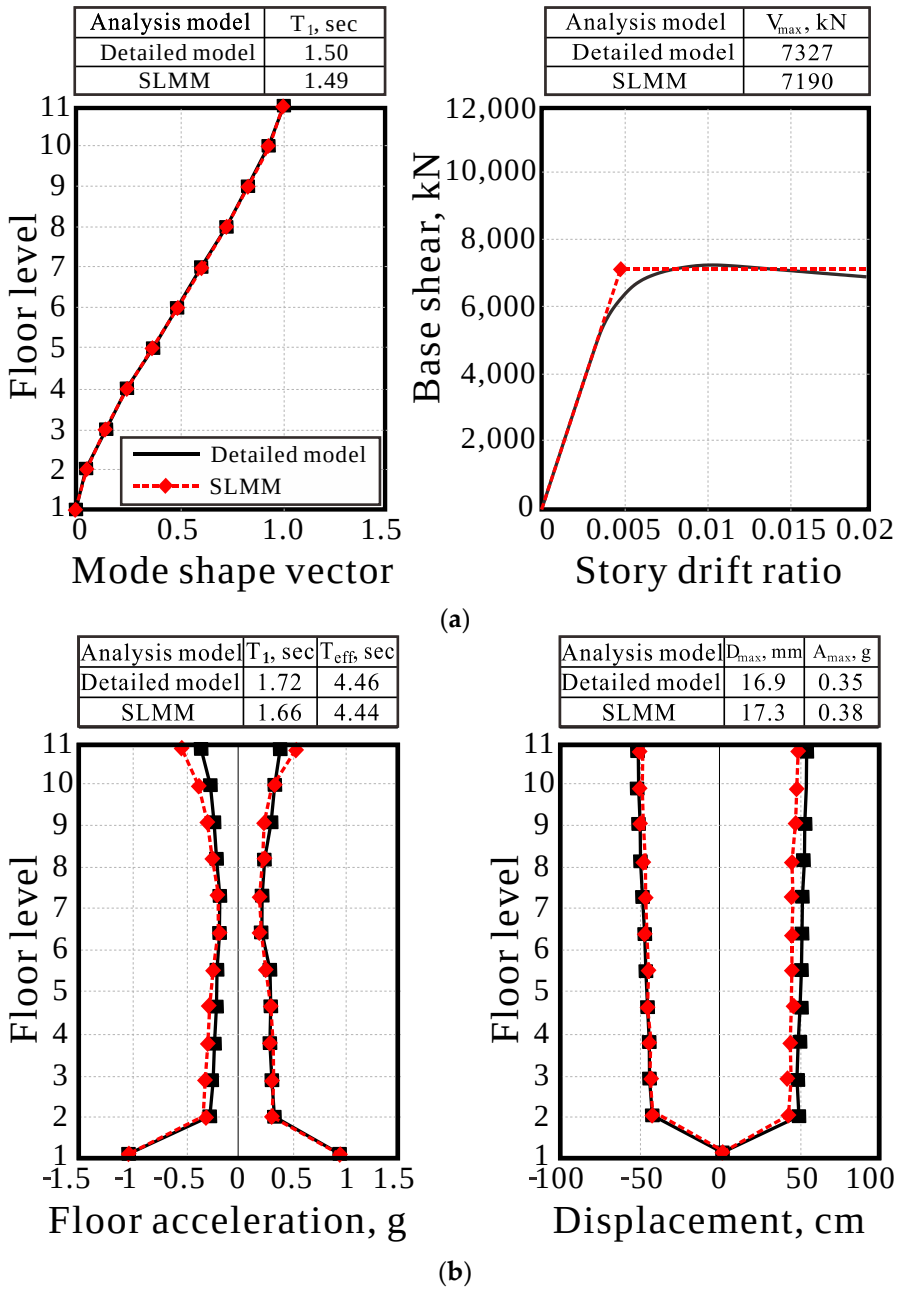

Figure 6. Comparison of analysis results of the simplified lumped mass model (SLMM) and the detailed model for $10L_E30B$ building: (**a**) Superstructures; (**b**) Isolated buildings.

Incremental dynamic analyses (IDAs) were performed with 40 ground motion records, which had been chosen from a far-field ground motion database provided by FEMA P695 [17]. The ground motion database includes a sufficient number of ground shaking records to permit evaluations of record-to-record variability that should be required for the calculations of median collapse intensity of a structure. A total of 40 ground motion records obtained from 20 earthquakes (two records for a single earthquake), as shown in Table 4, was used for uni-directional excitations. Records in the database had been already calibrated by normalizing their values of peak ground velocity (PGV) by the median PGV to reduce the inappropriate variability.

Table 4. Properties of selected historical ground motion records.

No. of EQ	Ground Motions	Stations	Duration, s	Magnitude	PGA, g	
					X-Comp	Y-Comp
1, 2	Northridge	Beverly Hills-Mulhol	29.99	6.7	0.416	0.516
3, 4	Northridge	Canyon Country-WLC	19.99	6.7	0.410	0.482
5, 6	Duze, Turkey	Bolu	55.9	7.1	0.728	0.822
7, 8	Hector Mine	Hector	45.31	7.1	0.266	0.337
9, 10	Imperial Valley	Delta	99.92	6.5	0.238	0.351
11, 12	Imperial Valley	El Centro Array #11	39.035	6.5	0.364	0.380
13, 14	Kobe, Japan	Nishi-Akashi	40.96	6.9	0.509	0.503
15, 16	Kobe, Japan	Shin-Osaka	40.96	6.9	0.243	0.212
17, 18	Kocaeli, Turkey	Duzce	27.185	7.5	0.312	0.358
19, 20	Kocaeli, Turkey	Arcelik	30	7.5	0.218	0.149
21, 22	Landers	Yermo Fire Station	44	7.3	0.245	0.152
23, 24	Landers	Coolwater	27.965	7.3	0.283	0.417
25, 26	Loma Prieta	Capitola	39.955	6.9	0.529	0.443
27, 28	Loma Prieta	Gilroy Array #3	39.945	6.9	0.555	0.367
29, 30	Superstition Hills	El Centro Imp.Co.	40	6.5	0.358	0.258
31, 32	Superstition Hills	Poe Road (temp)	22.3	6.5	0.446	0.300
33, 34	Cape Mendocino	Rio Dell Overpass	36	7.0	0.385	0.549
35, 36	Chi-Chi, Taiwan	CHY101	90	7.6	0.353	0.440
37, 38	San Fernando	LA-Hollywood Stor	28	6.6	0.210	0.174
39, 40	Friuli, Italy	Tolmezzo	36.345	6.5	0.351	0.315

According to the criteria in ASCE/SEI 7 [14], response spectral accelerations of the selected 40 accelerograms were scaled until the horizontal response spectra over the period range of $0.75T_{M,UB}$ to $1.25T_{M,LB}$ were equal to or greater than those of the MCE seismic hazard levels where $T_{M,UB}$ and $T_{M,LB}$ are the effective periods at maximum displacements which are determined using upper and lower bound properties. Figure 7 presents the mean response spectrum of scaled ground motions and target MCE spectrum of the prototype isolated buildings located at high and low-to-moderate seismicity regions.

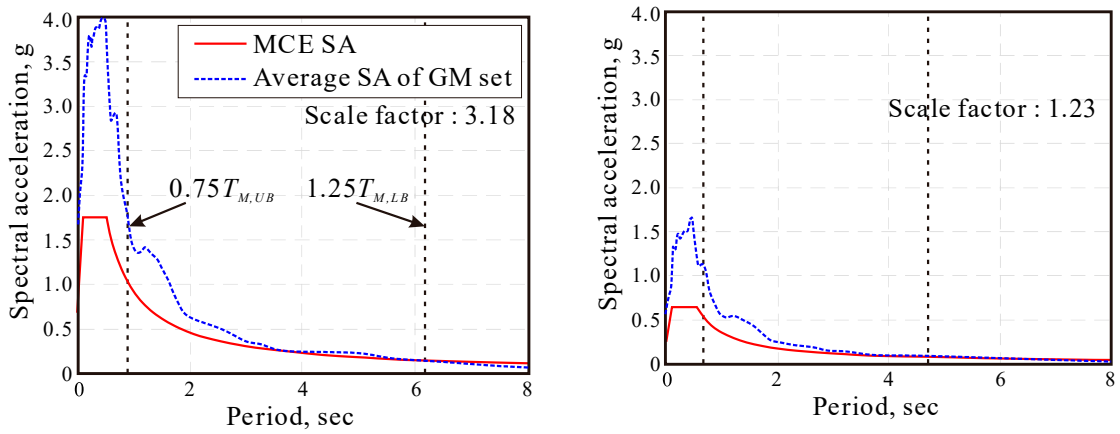

Figure 7. Response spectra of scaled earthquake records for prototype isolated buildings: (**a**) High seismicity regions; (**b**) Low-seismicity regions.

In this study, an isolated building is considered in the collapse state when they reach the limit states of both the superstructure and the isolation system. The limit states of the isolated buildings are determined according to the predefined criteria: (1) the maximum story drift of the superstructure exceeds the limit value of 0.04, (2) the maximum shear strain of the isolation system exceeds the limit value of 250%, or (3) the tangential slope calculated in the current step is less than 20% of the initial slop in a corresponding IDA curve. The collapse criterion in terms of a story drift ratio of 0.04 is

adopted from concrete frames of FEMA356 [29] and reinforced concrete moment resisting frames of HAZUS-MH [30]. Such collapse states of reinforced concrete frames include extensive cracking, splice failure in the nonductile column, and severe damage in short columns. Since excessive shear strains can cause problems such as the pounding and buckling, the allowable peak shear strain defined as the collapse state of isolation systems including LRBs and NRBs was conservatively set to 250% following the suggestion of Zhang and Huo [31], although modern elastomeric isolating bearing often withstands as much as 400% of the shear strain [32]. The allowable deformation of the FSBs is larger than that of LRB and NRB type isolators.

3.2. Collapse Capacity Evaluation of the Prototype Isolated Buildings

3.2.1. Results of Incremental Dynamic Analysis

Since isolated buildings should assure stable behaviors subjected to more severe earthquakes than conventional structures and their seismic performance is mainly dependent upon the cyclic behavior of the isolation systems, more rigorous evaluations for isolators are required. In this study, the structural capacities of the prototype isolated buildings were evaluated using the incremental dynamic analysis (IDA). The maximum story drifts of the superstructures and the maximum deformation of the isolation systems were observed with incremental earthquake intensities. The rigorous IDA methodology is based on the relation between the seismic response of a structure considered and the intensity levels of potential ground motion records. For the IDA procedure, this study implemented a hunt-and-fill algorithm that increases earthquake intensities until a structure reaches collapse. At a step finding the collapse of a structure, the process carries out backward filling between earthquake intensities in the previous steps [33]. The collapse points are defined as the spectral acceleration $S_a(T_M)$ at the effective period, T_M, of an isolated building at the collapse.

Figures 8 and 9 present the IDA curves of the prototype isolated buildings built at high and low-to-moderate seismicity regions, respectively. The slight, moderate, extensive, and collapse damage states presented in the figures are referred from HAZUS-MH [30]. In addition, the figures contain an earthquake record that the median collapse IDA curve is generated, and a collapse margin ratio (CMR) is defined as a ratio of a median collapse spectral acceleration to the MCE spectral acceleration, S_{MT}. Collapse points defined as a pair of the seismic demand and capacity are presented as scattered dots on the IDA curves. CMR values, median ordinates of scattered dots in the figures, of the prototype isolated buildings are significantly larger than 1.0 and are dependent on the critical failure modes of the isolated buildings. The CMR values of the isolated buildings located at low-to-moderate seismicity regions are larger than those at high seismicity regions. For the 3-story isolated buildings designed for high seismicity regions, $3S_E40C$ and $3S_E30B$ buildings in the figures, collapse points are collectively scattered around the collapse damage criteria for the maximum displacement of isolation systems, while collapse points gather far from the collapse damage criteria of the superstructures. This is demonstrated from the observation that at the collapse state, the superstructures experience slight or moderate damage states corresponding to 0.63% and 1.0% for story drift ratio rather than the collapse [30]. It is confirmed from this that the critical failure mechanism of the $3S_E40C$ and $3S_E30B$ buildings is the concentrated deformations at the isolators followed by the failure of isolation systems. These concentrated deformations at the isolation systems induce the pronouncing decoupling effect that let the superstructure almost behave as a rigid body (very small story drifts relative to isolator's displacements) and lower seismic energy transmitted. Similar observations are found on the 5- and 10-story isolated buildings, denoted as $5S_E40C$, $5S_E30B$, and $10S_E30B$ buildings in the figures, which are designed for high seismicity regions except for the $10S_E40C$ building where the governing collapse mode is determined by lateral displacements of the superstructure. The larger structural period of the tall $10S_E40C$ building causes the decoupling effects to vanish.

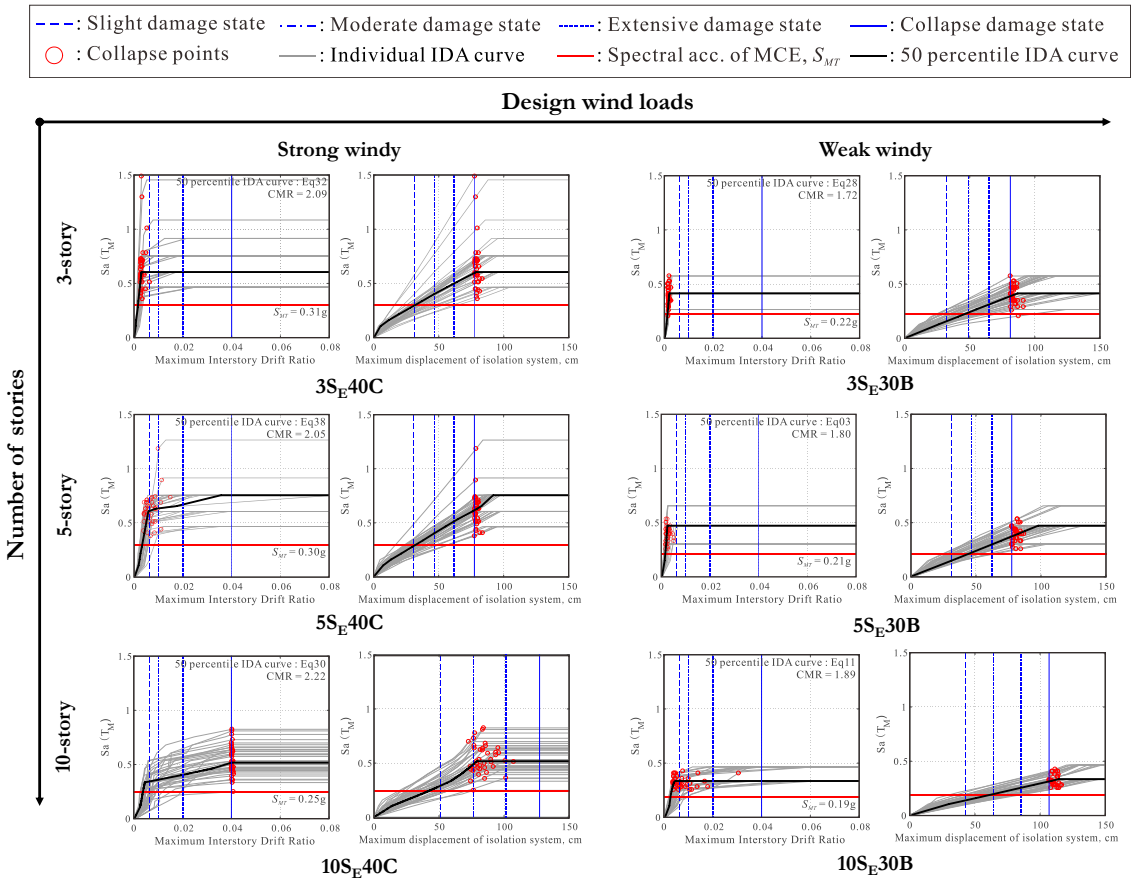

Figure 8. IDA curves for isolated buildings located at high seismicity regions.

For the prototype isolated buildings designed for low-to-moderate seismicity regions especially for strong windy regions, 3L$_E$40C, 5L$_E$40C, and 10L$_E$40C buildings in the figures, the superstructures are in the collapse damage state, resulting from large side-sway displacements. On the other hand, the isolation systems do not reach the collapse damage state. Hence, the distributions of the collapse points are concentrated near the collapse damage criterion in terms of the maximum story drift ratio of the superstructure, as presented in Figure 9. At the collapse state, the isolation systems in the 3L$_E$40C building suffer the extensive damage defined as 200% of shear strains [31]. The isolation systems in the 5L$_E$40C and 10L$_E$40C buildings are approximately in the moderate and slight damage states, respectively when the corresponding superstructures reach the collapse damage state. This results from the loss of the beneficial decoupling effects that should expect to be developed in the L$_E$40C buildings. This phenomenon is magnified as their heights are increased. Of the L$_E$30B buildings subjected to smaller design wind loads, the 3L$_E$30B building develops the promising decoupling effects, whose damage is concentrated on the isolators. Both the 5L$_E$30B and 10L$_E$30B buildings suffer significant structural damage on the superstructure rather than the isolators.

The several IDA curves show the structural resurrection in which response is again stiffer at larger ground motion intensities after a flattened response at a particular ground motion intensity. The structural resurrection is also found in the IDA curves presented in terms of the story drift ratio of the superstructure. Such structural resurrection contributing the larger variation on IDA curves is notable to isolated buildings, which commonly capture the critical failures due to the side-sway of the superstructures. With the resurrection, the dispersion of collapse points is mainly dependent on seismic design conditions of isolated buildings. The larger dispersions are observed for isolated buildings designed for low seismicity regions compared to those for high seismicity regions. Similar findings are also observed for taller isolated buildings under larger design wind loads. The fragility curve of each

prototype isolated building was determined from a cumulative distribution function (CDF) of collapse points on its IDA curve with an assumption that they follow the well-known log-normal distribution characterized by two parameters, a median and a standard deviation. Record-to-record uncertainties can be directly quantified by the logarithmic standard deviation of a distribution. Based on these probabilistic parameters, the fragility curves of the isolated buildings considered in this study are found in Figure 10.

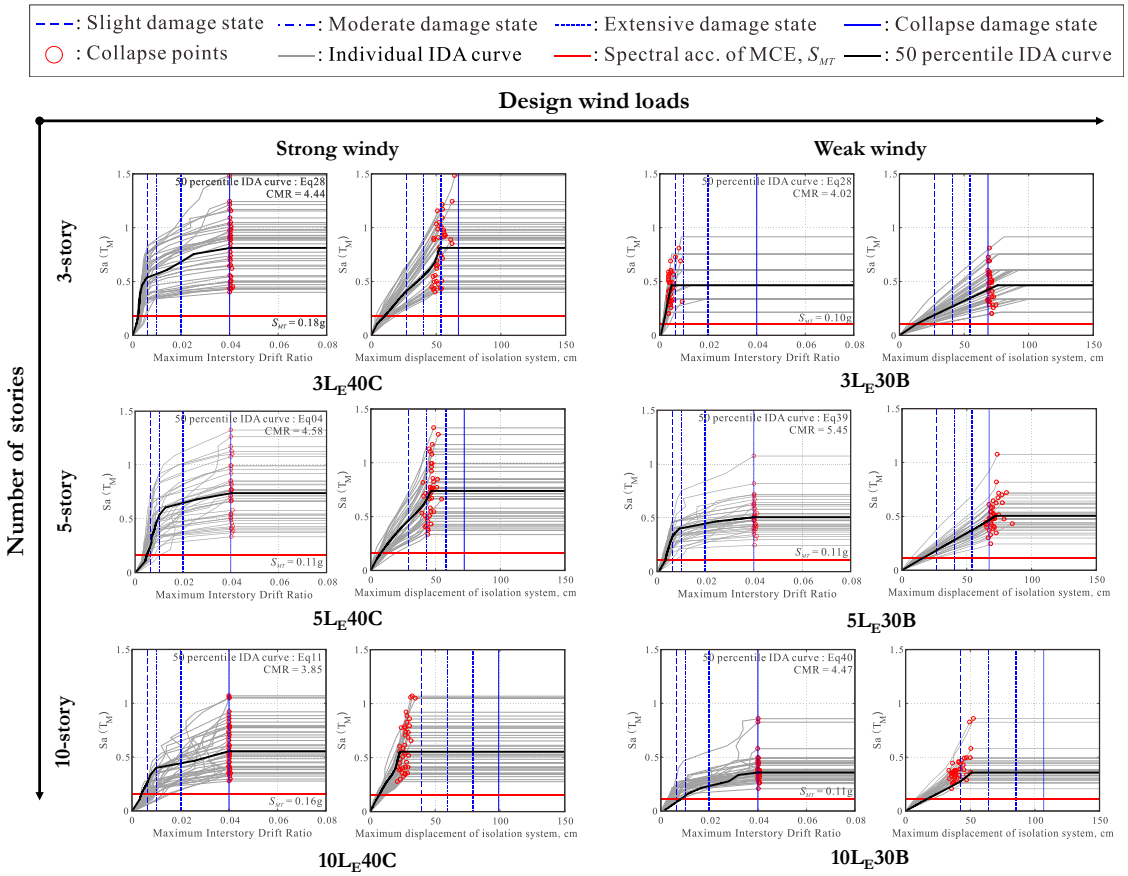

Figure 9. Incremental dynamic analyses (IDA) curves for isolated buildings located at low-to-moderate seismicity regions.

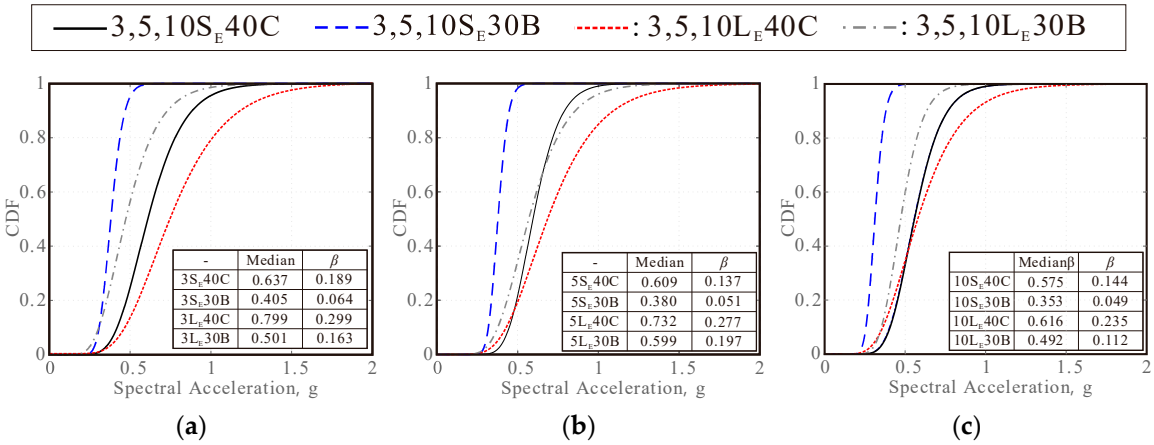

Figure 10. Fragility curves of prototype isolated buildings: (**a**) 3-story; (**b**) 5-story; (**c**) 10-story.

3.2.2. Assessment of Probabilistic Propagation of Modeling Uncertainty Sources Related to Isolated Buildings

There are various sources resulting variations on the seismic response of a structural system [34]. Uncertainties are typically classified into record-to-record uncertainties, modeling uncertainties, design requirement uncertainties, and test data uncertainties. Of them, record-to-record variability can be, as mentioned above, quantitatively evaluated from IDA results that can be obtained by repeated seismic analyses of structures using various ground motion records. Design requirement-related uncertainty and the test data uncertainty can be quantified in terms of their quality rating in accordance with requirements in FEMA P695 [17].

Modeling uncertainty can be determined from Monte-Carlo simulation based-evaluation which is carried out with statistical information on material properties and analytical assumption. Table 5 summarizes the statistical information on modeling uncertainties that are treated as random variables categorized into four structural properties of a superstructure and isolators (denoted as *SSP* and *ISP* in the table), inherent damping ratios (denoted as *DP* in the table), and gravity loads (denoted as *GL* in the table). This table contains bias factors and the coefficient of variation of each random variable obtained from corresponding references. As shown in Figures 8 and 9, record-to-record uncertainty is an important factor influencing the structural capacities of the prototype isolated buildings. Such record-to-record uncertainty should be eliminated in order to concentrate on the effects of random variables related to the modeling uncertainty. Using the IDA results that are carried out for the prototype isolated buildings, a representative ground motion record is selected as one where the median collapse point is measured. The representative ground motion record of each prototype building can be found in Figures 8 and 9. The four categorized modeling uncertainties are randomly selected from their probabilistic distributions. Generating representative sample sets of modeling uncertainties was comprised using a Latin hypercube sampling method. Since the error rate of Monte Carlo simulation is changed by a sample size, a required minimum sample size was first evaluated. The sampling size was determined by the convergence tests shown in Figure 11. The sampling for the convergence test was continuously performed until a ratio between the mean (or standard deviation) of a sample set and the mean (or standard deviation) of the population is less than a tolerance.

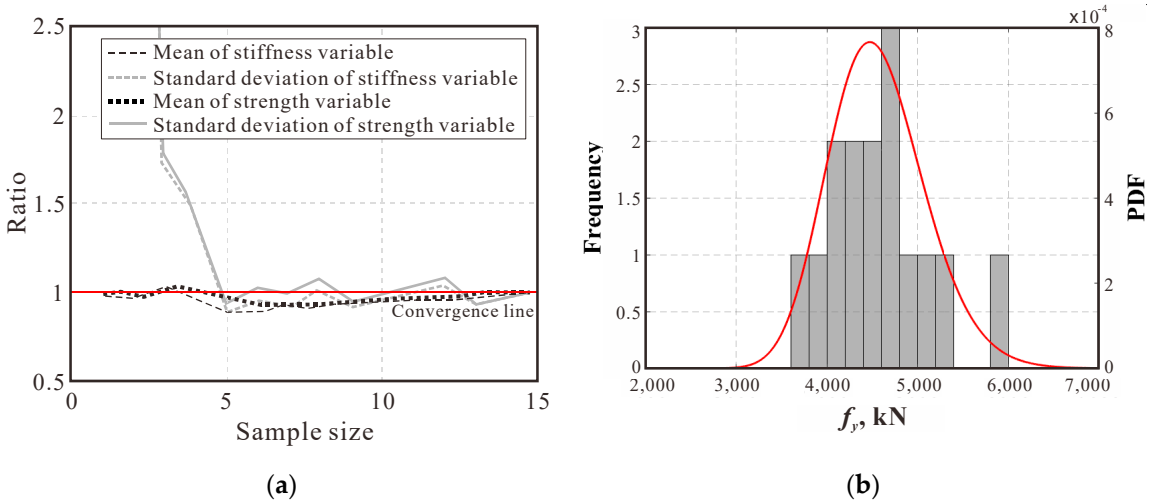

Figure 11. Sampling of modeling uncertainty (example values f_y in SSP for $3S_E40C$): (**a**) Latin hypercube sampling; (**b**) Convergence test for f_y values.

Table 5. Statistical information on sources related to the modeling uncertainty.

Category	Random Variables	Distribution Type	λ	δ	Reference
SSP	f_{ck} f_y	Normal Log-Normal	1.14 1.05	0.18 0.11	Ellingwood et al. [35], Celik and Ellingwood [36]
DP	D_p	Log-Normal	1.0	0.30 to 0.40	Porter et al. [37]
ISP	K_{NRB} K_{LRB} Q_{LRB}	Uniform Uniform Uniform	1.0 1.0 1.0	0.8μ to 1.8μ 0.8μ to 1.8μ 0.8μ to 1.8μ	ASCE/SEI 7 [14], Han et al. [32]
GL	*D.L.* *L.L.*	Normal Gumbel	1.05 Varies per floor area	0.10 0.25	Ellingwood et al. [35]

Note: *SSP*: structural properties related to the superstructure, *DP*: inherent damping ratio of the isolated structures, *ISP*: structural properties related to the hysteresis behavior of isolation system, *GL*: gravity load, f_{ck}: compressive strength of concrete material, f_y: yield strength of reinforcements, K_{NRB}: stiffness of natural rubber bearing, K_{LRB}: stiffness of lead rubber bearing, Q_{LRB}: yield strength of lead rubber bearing, *D.L.*: dead load, *L.L.*: live load, λ: bias factor of the random variable, δ: coefficient of variation of the random variable.

Figure 12 shows the IDA curves of the 5L$_E$40C building subjected to the representative ground motion record. The variation of the IDA curves results from the modeling uncertainties due to variations of the four categories (*SSP*, *ISP*, *DP*, and *GL*). The figure clearly shows the dominance of the modeling uncertainty propagation on story drift variance rather than isolation displacement variance. Such behavior is particularly found in the IDA curves of the prototype buildings of which the collapse damage state is determined by the sideway of the superstructure. The variations of seismic capacities $S_a(T_M)$ induced by the modeling uncertainties are comparatively evaluated in a format of tornado diagrams, as shown in Figure 13. The horizontal axis in the figure indicates the normalized variation ratios $\hat{\varepsilon}_{SA}$ of $S_a(T_M)$ values. The $\hat{\varepsilon}_{SA}$ value is determined by dividing ±2 standard deviation dispersion by the median value. Of the four categories chosen for considering the modeling uncertainties in this study, variance of the *ISP* is the most dominant contributor on the variations of $\hat{\varepsilon}_{SA}$. A *GL* variance is positively correlated, while variances of the *SSP* and *DP* are negatively correlated with the output random variable, $\hat{\varepsilon}_{SA}$, of the prototype isolated buildings, which can be confirmed from Figure 12. Table 6 summarizes the lognormal standard deviation parameter, β_{MDL} of the modeling uncertainty derived from the square-root-of-sum-of-squares (SRSS) combination of the standard deviations of the four categories. In consequence, the prototype isolated buildings located at strong seismicity regions present lower probabilistic propagations of the modeling uncertainty in comparison to those located at low-to-moderate earthquake regions. According to the design wind loads considered, probabilistic propagations of modeling uncertainties are more influential to the seismic capacity of the prototype isolated buildings at strong windy regions than those at weak windy regions. This is pronounced for taller isolated buildings required the larger $\Delta F_{R,req}$.

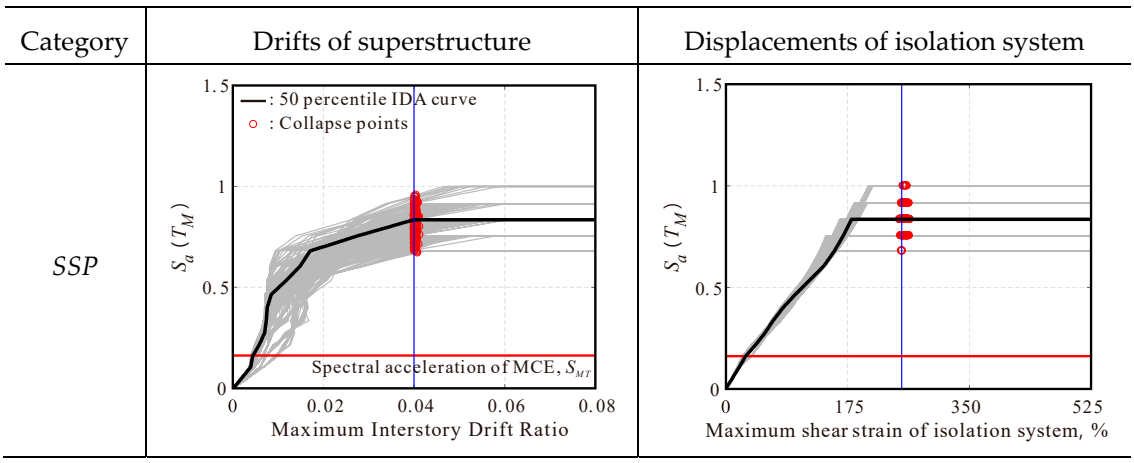

Figure 12. *Cont.*

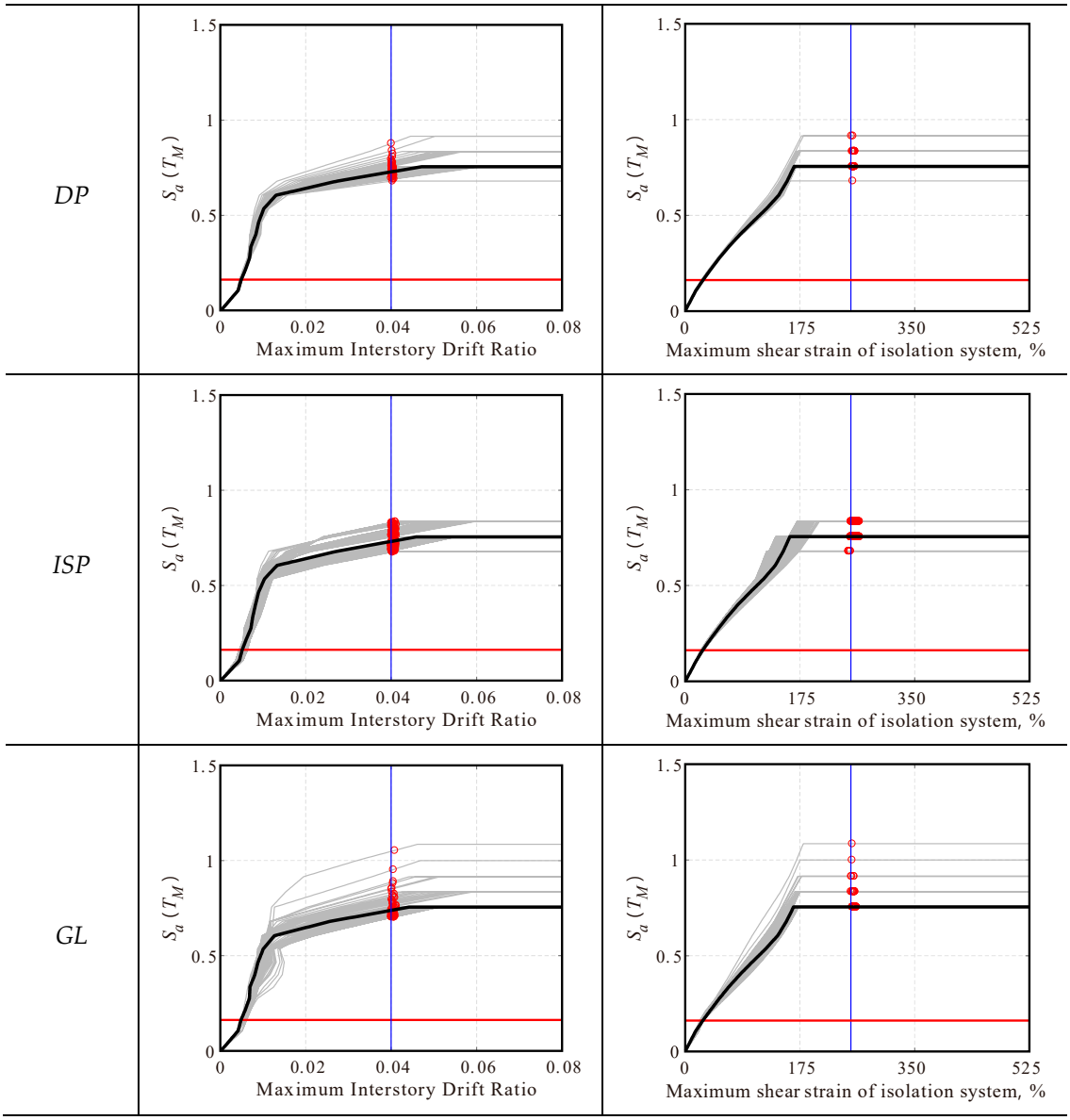

Figure 12. Modeling uncertainty propagations to IDA curves of 5LE40C.

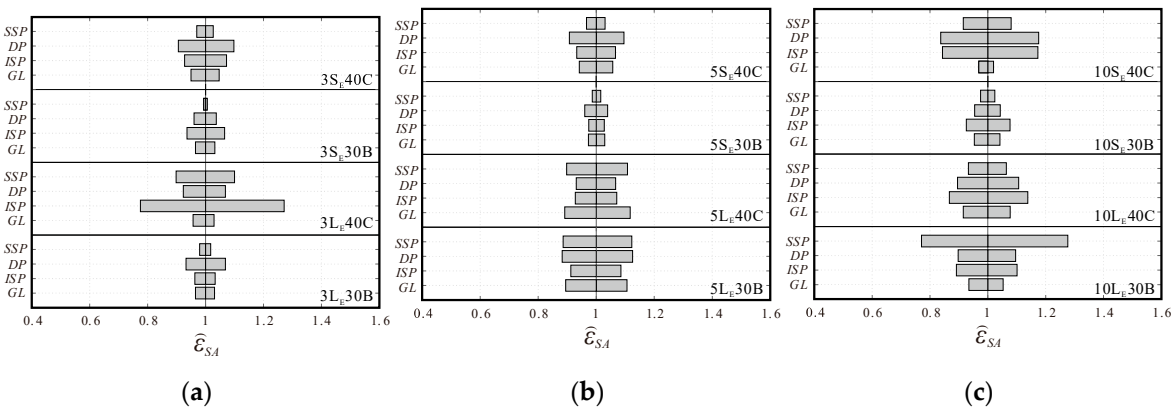

Figure 13. Sensitivity analysis of modeling uncertainty of prototype buildings: (**a**) 3-story; (**b**) 5-story; (**c**) 10-story.

Table 6. Lognormal standard deviation parameter of the modeling uncertainty.

(a) Buildings at High Seismicity Regions						
-	**Strong Windy Region**			**Weak Windy Region**		
	3S$_E$40C	**5S$_E$40C**	**10S$_E$40C**	**3S$_E$30B**	**5S$_E$30B**	**10S$_E$30B**
β_{MDL}	0.064	0.069	0.109	0.020	0.011	0.025
(b) Buildings at Low-to-Moderate Seismicity Regions						
-	**Strong Windy Region**			**Weak Windy Region**		
	3L$_E$40C	**5L$_E$40C**	**10L$_E$40C**	**3L$_E$30B**	**5L$_E$30B**	**10L$_E$30B**
β_{MDL}	0.187	0.113	0.108	0.029	0.089	0.093

4. Comparative Evaluation of Collapse Probability

4.1. Methodology to Evaluate Collapse Probability

Several researchers indicated that the spectral shape of ground motion imposed to a structure, in addition to its intensity, is important to evaluate seismic structural response [38,39]. In particular, for a given seismic hazard level, the uniform hazard spectrum can be quite different from the shapes of the expected response spectra of real ground motion having a fluctuated spectral amplitude at a single period of interest. These spectral shape characteristics are especially important for the seismic collapse evaluation of a structure in that these differences can be significantly amplified at high amplitudes [40].

A simple procedure for accounting for the spectral shape effects is described on FEMA P695 [17] for non-isolated concrete and/or wood frames with relatively short structural periods. It is questionable to apply this procedure to seismically isolated buildings of which the collapse mechanisms can be developed at the isolation systems rather than the superstructures and, in turn, the fundamental periods are large. In this study, the collapse evaluations of the prototype isolated structures are carried out according to Haselton et al. [40] that can directly consider the spectral shape effects in a structure with the relatively large structural period. As shown in Figure 14, the acceleration spectra of an individual ground motion have much different shapes from the uniform hazard spectrum. In this study, the acceleration spectrum used in designing the prototype structures is assumed as the uniform hazard spectrum. The spectral shape effects are represented by a parameter of ε that graphically means the difference between an individual ground motion spectrum and a uniform hazard spectrum excluding the variation of earthquake waveforms. Larger ε values of a typical individual spectrum usually exist approximately less than 2.0 s. Unlike typical structural systems with relatively short fundamental periods, values of ε for isolated buildings would be smaller. A value, $\varepsilon_j(T_M)$ at T_M of the jth ground motion record (j ranges from 1 to 40) is a coefficient of variance of a random variable of spectral acceleration at a period of T_M and is obtained from:

$$\varepsilon_j(T_M) = \frac{\ln\left[S_{aj}(T_M)\right] - \mu_{\ln Sa}(T_M)}{\sigma_{\ln Sa}(T_M)} \quad (1)$$

where $S_{aj}(T_M)$ is a spectral acceleration at T_M of the jth ground motion record, and $\mu_{\ln Sa}(T_M)$ and $\sigma_{\ln\ Sa}(T_M)$ are, respectively, the mean and standard deviation of spectral accelerations at T_M of the ensemble of ground motion records. Values of $\sigma_{\ln\ Sa}(T_M)$ for the ensembles of earthquake records representing high and low-to-moderate seismicity regions are 0.64 and 0.45, respectively [41,42]. Values of ε dependent upon the site and hazard level need to be calibrated to obtain a representative spectral shape so that a target (or expected) ε value, denoted as $\bar{\varepsilon}_0$, is generally introduced. The value of $\bar{\varepsilon}_0$ for the building response assessment can be obtained from the de-aggregation of ground motion hazard (probabilistic seismic hazard analysis) for a specific location, site class, spectral period, and return period. According to the USGS (United States Geological Survey) website [43] providing

the information of high and low-to-moderate seismicity regions, the values of $\bar{\varepsilon}_0$ at the fundamental period, T_M, for MCE records can be obtained. The values of $\bar{\varepsilon}_0$ for the prototype isolated buildings are summarized in Table 7.

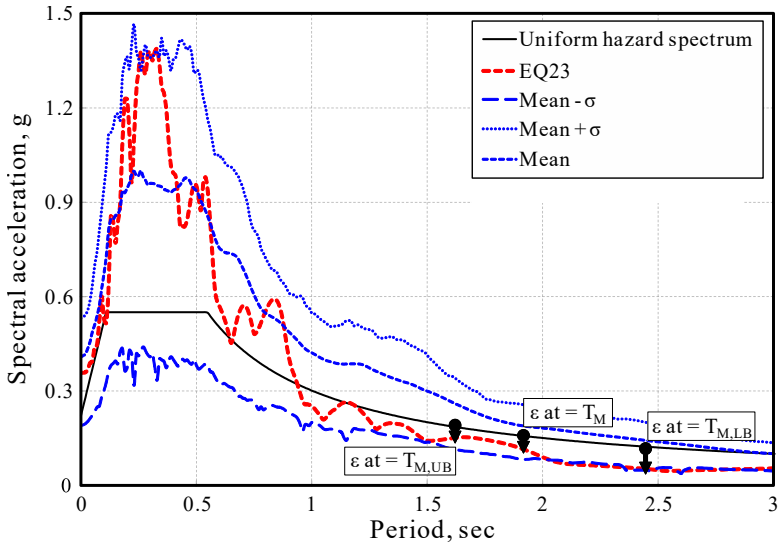

Figure 14. Comparison of an observed spectrum (EQ23) with uniform hazard spectrum.

Table 7. Results of collapse probability evaluation for prototype isolated buildings.

Design Condition	Prototype Buildings	Median Collapse Spectral Acceleration					Collapse Probability		
		ε_0	c_0	c_1	$S_{a,Col,adj}$, g	$S_{a,MCE}$, g	β_{TOT}	*ACMR*	$P_{COL,MCE}$, %
Buildings at high seismicity region	$3S_E40C$	1.544	−0.6246	0.0793	0.605	0.305	0.257	1.984	0.38
	$5S_E40C$	1.537	−0.8953	0.1644	0.526	0.297	0.210	1.771	0.32
	$10S_E40C$	1.479	−1.1852	0.2665	0.453	0.245	0.229	1.851	0.36
	$3S_E30B$	1.446	−1.1723	0.1023	0.359	0.224	0.159	1.603	0.15
	$5S_E30B$	1.423	−1.2973	0.1414	0.334	0.211	0.158	1.584	0.18
	$10S_E30B$	1.370	−1.3105	0.0574	0.292	0.187	0.154	1.560	0.19
Buildings at low-to-moderate seismicity region	$3L_E40C$	0.808	−1.2594	0.1803	0.328	0.180	0.380	1.824	5.69
	$5L_E40C$	0.809	−1.4851	0.2101	0.268	0.162	0.334	1.657	6.53
	$10L_E40C$	0.809	−1.5954	0.2075	0.240	0.158	0.293	1.518	7.71
	$3L_E30B$	0.818	−1.9169	0.2590	0.182	0.109	0.217	1.667	0.93
	$5L_E30B$	0.817	−1.8140	0.1880	0.190	0.110	0.255	1.728	1.60
	$10L_E30B$	0.817	−1.8721	0.1526	0.174	0.110	0.247	1.584	3.13

With the consideration of the spectral shape effects mentioned above, the median collapse spectral acceleration is calculated by the following steps [24]:

(1) Perform incremental dynamic analysis to obtain the collapse capacity defined as the spectral acceleration $S_{a,Col,j}(T_M)$ at the collapse under the jth ground motion;

(2) Calculate $\varepsilon_j(T_M)$ at T_M using Equation (1);

(3) Perform a linear regression analysis between $\ln\left[S_{aj}(T_M)\right]$ and $\varepsilon_j(T_M)$, as shown in Figure 15, and determine coefficients c_0 and c_1 (summarized in Table 7) from the following equation:

$$\ln\left[S_{a,Col}(T_M)\right] = c_0 + c_1\varepsilon(T_M); \quad (2)$$

(4) Replace $\varepsilon(T_M)$ with $\bar{\varepsilon}_0(T_M)$ in Equation (2) and obtain an adjusted median collapse capacity, $\hat{S}_{a,Col,adj}(T_M)$:

$$\hat{S}_{a,Col,adj}(T_M) = \exp\left[c_0 + c_1\bar{\varepsilon}_0(T_M)\right]; \quad (3)$$

(5) Compute adjusted collapse margin ratios (ACMR) using the equation:

$$ACMR = \frac{\hat{S}_{a,col,adj}(T_M)}{S_{a,MCE}(T_M)}; \quad (4)$$

(6) Calculate the conditional probability of the collapse caused by MCEs, $P_{Col,MCE}$ using the equation:

$$P_{COL,MCE} = \int_0^1 \frac{1}{s\beta_{TOT}\sqrt{2\pi}} \exp\left[\frac{(\ln s - \ln ACMR)^2}{2\beta_{TOT}^2}\right] ds. \quad (5)$$

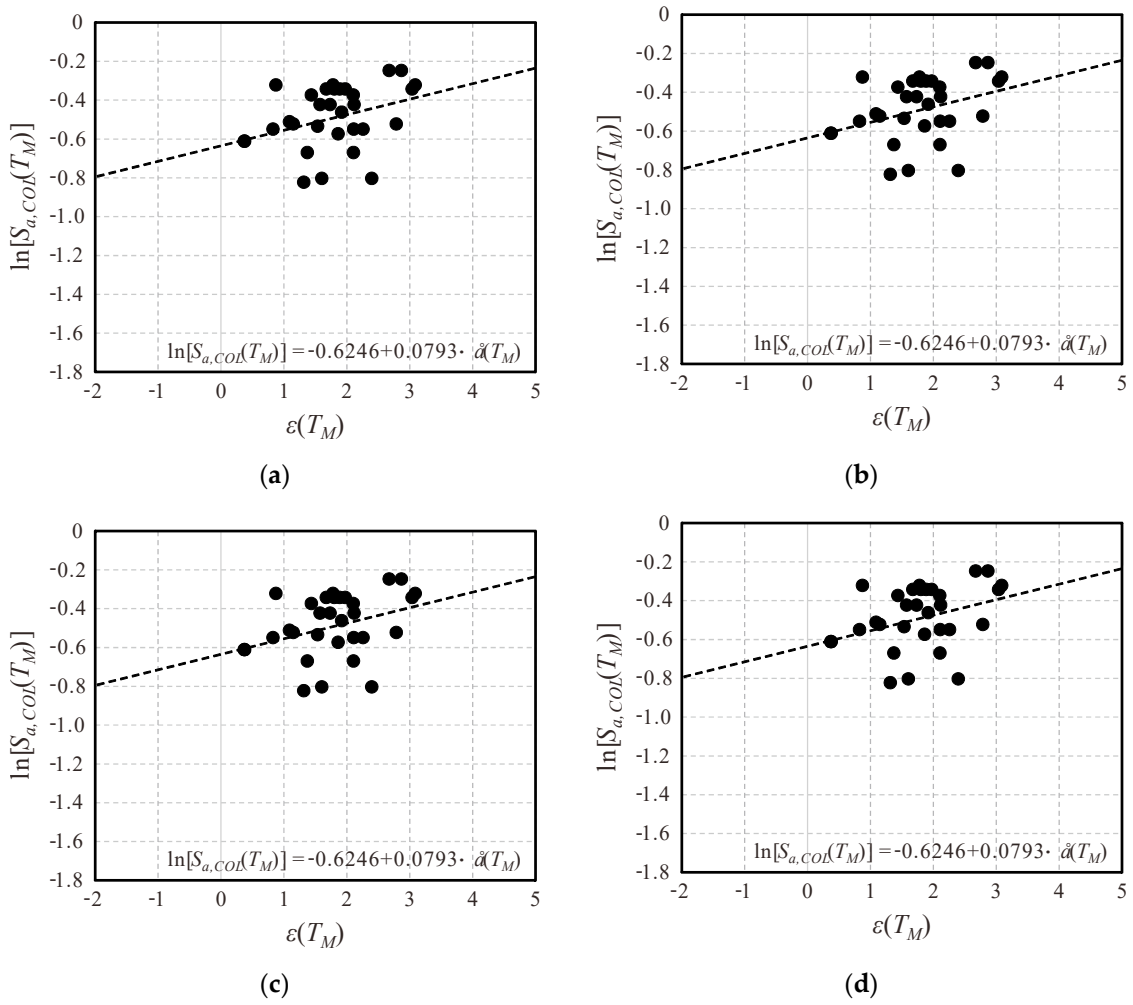

Figure 15. Sample relations between ln[$S_{aCol,i}(T_M)$] and $\varepsilon_j(T_M)$: (**a**) 3S_E40C; (**b**) 3S_E30B; (**c**) 3L_E40C; (**d**) 3L_E30B buildings.

The equation for $P_{Col,MCE}$ includes the probabilistic propagation of uncertainty sources to the collapse capacities of an isolated building. It is assumed that each uncertainty is independent and lognormally distributed with a median value and lognormal standard deviation. The total uncertainty in the equation, β_{TOT}, is calculated by the SRSS combination of a design requirement-related uncertainty, β_{DR}, a test-data related uncertainty, β_{TD}, a modeling-related uncertainty, β_{MDL}, and a record-to-record collapse uncertainty, β_{RTR}. Among uncertainty sources, β_{MDL} and β_{RTR} are pre-determined from the incremental dynamic analysis results of the prototype isolated structures. For isolated buildings designed according to a current seismic code, their rigorous design requirements should be followed

including strict prototype testing procedures, and their excellent seismic performance has been supported by explicit academic investigations against MCE ground motion and seismic renaissance reports. Hence, a value of β_{DR} for the design requirements for isolated buildings can be rated as superior, β_{DR} =1.0. Regarding the test-data related uncertainty, test data related to both superstructure components such as the RC beam, column and beam-column joint, and to isolation systems shall be considered. From a large number of previous research studies related to reinforced concrete components, various experimental verifications are carried out for structural components in RC moment-resisting frames. With prototype tests for representative isolation systems to be employed into building construction, the production test of every single isolator should be also carried out to ensure its cyclic behavior. Thus, since all isolation systems should be experimentally verified, substantially low uncertainty related to test data can be guaranteed and a value of β_{TD} is also rated as superior, β_{TD} =1.0. Finally, the values of $P_{Col,MCE}$ and β_{TOT} of the prototype isolated buildings are calculated and summarized in Table 7.

4.2. Discussion on the Collapse Probability of Prototype Isolated Buildings

In order to evaluate the seismic performance of a building according to the performance objectives, more specific criteria are required to determine whether or not they are attainable. As a part of carrying out the probability-based evaluation of an isolated building, the target reliability should be established as a quantitative value defined as the conditional probability of the collapse. Since the target reliability depends on the risk category of a building prescribed on a current seismic code, this study sets the required conditional collapse probabilities against the MCE seismic intensity not to exceed 3% for the prototype isolated structures. Note that isolators are usually implemented for essential buildings of the risk category IV falling into important facilities of which the failure could pose a substantial hazard to the community. These target reliabilities should be compared with the calculated probability of collapse presented in Table 7.

It could be expected in the design phase that the collapse probabilities of the prototype isolated buildings under future MCEs are lower than the required maximum conditional collapse probability of 10% for typical buildings. Values of $P_{Col,MCE}$ in Table 7 demonstrates that all prototype buildings designed according to the current seismic design procedure well satisfy this expectation. However, the table also shows that the maximum $P_{Col,MCE}$ value of 7.71% is found at the $10L_E40C$ building, while the minimum value of 0.15% is calculated at the $3S_E30B$ building. Such a huge difference in $P_{Col,MCE}$ should be minimized to achieve similar reliabilities for every isolated building, regardless of its design conditions.

The prototype isolated buildings designed for high seismicity regions, the S_E buildings, possess very small values of $P_{Col,MCE}$ less than 1%, which is still smaller than the acceptable conditional collapse probability of 3% against the MCE earthquake intensity. The fundamental periods, T_M, of the S_E buildings are considerably larger than 2.5 s, and their collapse mode is dominated by the concentrated displacements on isolators with the undamaged state on their superstructures. For buildings with larger values of T_M, the inelastic action of their superstructures is eliminated, and the isolators suffer most of the displacement demands. This simple mechanism causes the decrease in uncertainty propagations to the seismic responses of the S_E buildings and, consequently, leads to lower MCE collapse probabilities that those of the L_E buildings with similar ACMR and β_{TOT} values. Of the L_E buildings designed with smaller seismic loads, the L_E40C buildings built at strong windy regions present unacceptably high MCE collapse probabilities that are larger than 3%. The $10L_E30B$ building also develops the higher MCE collapse probability. Excessive stiffening behavior of their isolators in most of the buildings causes ratios of T_1/T_M larger than 0.35, which results in the loss of decoupling effects and the increase in seismic energy dissipation by the superstructure. This more complicated mechanism leading to the increase in uncertainty propagations increases the MCE collapse probabilities of the L_E buildings.

As mentioned earlier, even if the ACMR values of the L_E buildings are quantitatively similar to those of the corresponding S_E buildings, the MCE collapse probabilities dependent upon the governing

collapse mechanism are quite different. In a probabilistic concept, the most influential parameter including the unacceptable collapse probability of the L_E buildings is presumed as the total system uncertainty, β_{TOT}, which mainly depends on the dominant collapse modes developed by the structural systems. Figure 16 presents the calculated MCE collapse probabilities of the L_E buildings according to the changes of β_{TOT} required at the probabilistic calculation of Equation (5). This figure also provides the acceptable uncertainty of total system, $\beta_{TOT,A}$, that satisfies the target reliability resulting in the sufficient margin for the MCE collapses of isolated buildings. The improvement in the confidence level of isolated buildings designed according to a current seismic code can be intuitively achieved throughout the reduction in β_{TOT} values. A value of $\beta_{TOT,A}$ becomes the largest value of β_{TOT} of an isolated building of which the target MCE collapse probability reaches 3%. The MCE collapse probability of the $10L_E30B$ building becomes acceptable with only a small calibration of β_{TOT}. However, for the L_E40C buildings presenting unacceptably higher MCE collapse probabilities, the values of β_{TOT} are decreased to at least 0.75. Furthermore, a value of $\beta_{TOT,A} = 0.60$ is proposed to achieve a similar MCE collapse probability to the S_E buildings built at high seismicity regions.

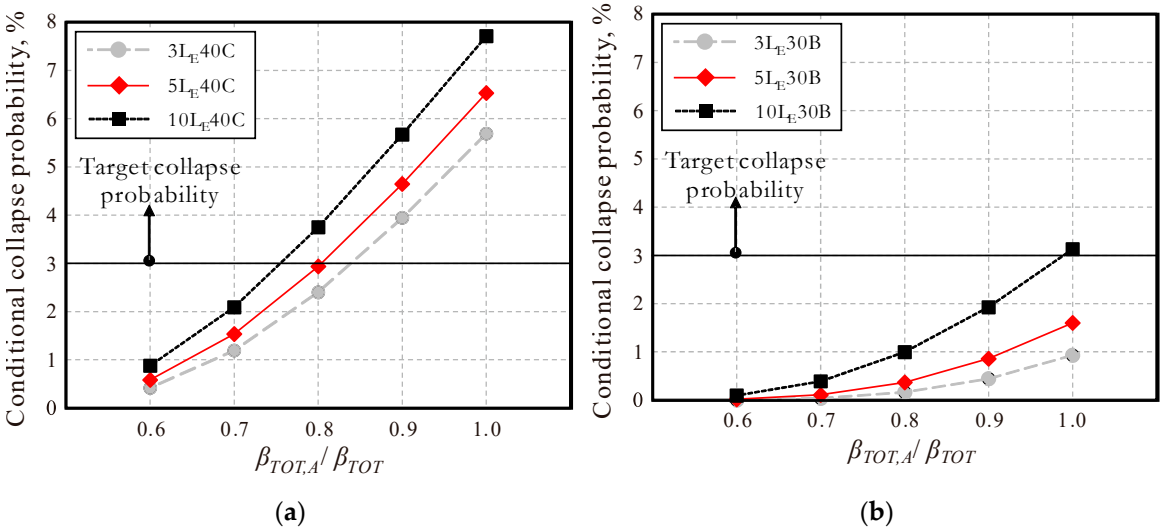

Figure 16. Collapse probabilities of isolated buildings located in low-to-moderate seismicity considering required total system uncertainty: (**a**) L_E40C buildings; (**b**) L_E30B buildings.

5. Conclusions

As a result of little information on the seismic performance of isolated buildings located at low-to-moderate seismicity regions, it is questionable that their collapse capacities can be ensured with reasonable reliability, although they would be designed according to a current seismic design code. This paper evaluates the MCE collapse capacities of the selected prototype isolated buildings throughout nonlinear incremental dynamic analyses. The important influential factors on the collapse probabilities of the prototype isolated buildings are quantified to specifically suggest the potential modifications of the design requirements.

The analysis results are presented in terms of their collapse capacities, including possible uncertainties. Although the MCE collapse probabilities of all prototype isolated buildings are smaller than those expected for typical non-isolated buildings, these values are significantly different according to the degree of seismicity. The MCE collapse probabilities are dependent upon the governing collapse mechanism and the total system uncertainty. For the prototype buildings located at low-to-moderate seismicity regions, 0.60 is proposed for $\beta_{TOT,A}$ to achieve a similar MCE collapse probability to the corresponding buildings built at high seismicity regions.

From the evaluation of the MCE collapse probability, the design requirements for isolated buildings located at low-to-moderate seismicity regions should be improved to guarantee the code-confirming

confidence level to high-risk categorized seismically important buildings. Modifications of the design requirements influencing the collapse mode of isolated buildings are carried out to ensure the promising decoupling mechanism of isolated systems. Specifically, lower post-yield stiffness ratios of isolation systems can be recommended in considering their smaller deformation demands under low-to-moderate seismicity. This can be also done by modifying property modification factors of an isolation system and eventually decreasing total system uncertainty, which is investigated by further studies carried out by the authors.

Author Contributions: Original draft manuscript, H.-J.K.; supervision and review writing, D.-H.S. All authors have read and agreed to the published version of the manuscript.

Funding: This work was supported by the 2018 Research Fund of the University of Seoul.

Acknowledgments: We gratefully acknowledge the support of University of Seoul.

Conflicts of Interest: The authors declare no conflict of interest.

References

1. Skinner, R.I.; Robinson, W.H.; McVerry, G.H. *An Introduction to Seismic Isolation*; John Wiley & Sons Inc.: New York, NY, USA, 1993.
2. Naeim, F.; Kelly, J.M. *Design of Seismic Isolated Structures: From Theory to Practice*; John Wiley and Sons Inc.: New York, NY, USA, 1999.
3. Jangid, R.S.; Datta, T.K. Seismic behavior of base isolated building: A state-of-the-art review. *Struct. Build.* **1995**, *110*, 186–203. [CrossRef]
4. Lin, A.N.; Shenton, H.W. Seismic performance of fixed-base and base-isolated steel frames. *J. Struct. Eng.* **1992**, *119*, 921–941. [CrossRef]
5. Furukawa, S.; Sato, E.; Shi, Y.; Becker, T.; Nakashima, M. Full-scale shaking table test of a base-isolated medical facility subjected to vertical motions. *Earthq. Eng. Struct. Dynam.* **2013**, *42*, 1931–1949. [CrossRef]
6. Nagarajaiah, S.; Reinhorn, A.M.; Constantinou, M.C. Torsion in base-isolated structures with elastomeric isolation systems. *J. Struct. Eng.* **1993**, *119*, 2932–2951. [CrossRef]
7. Zhou, Z.; Wong, J.; Mahin, S. Potentiality of using vertical and three-dimensional isolation systems in nuclear structures. *Nucl. Eng. Technol.* **2016**, *48*, 1237–1251. [CrossRef]
8. Katsaras, C.; Panagiotakos, T.; Kolias, B. Evaluation of current code requirements for displacement restoring capability of seismic isolation systems. In *Lessloss Risk Mitigation for Earthquakes and Landslides*; Project No: GOCE-CT-2003-505488; Pavia University: Pavia, Italy, 2006.
9. Mazza, F. Effects of the long-term behaviour of isolation devices on the seismic response of base-isolated buildings. *Struct. Control Health Monit.* **2019**, *26*, e2331. [CrossRef]
10. Kumar, M.; Whittaker, A.S.; Constantinou, M.C. An advanced numerical model of elastomeric seismic isolation bearings. *Earthq. Eng. Struct. Dyn.* **2014**, *43*, 1955–1974. [CrossRef]
11. Islam, A.B.M.S.; Ahmad, S.I.; Jameel, M.; Zamin, M.J. Seismic base isolating for buildings in regions of low to moderate seismicity: Practical alternative design. *Pract. Period. Struct. Des. Constr.* **2012**, *17*, 13–20. [CrossRef]
12. Martelli, A.; Forni, M. Seismic isolation of civil buildings in Europe. *Prog. Struct. Eng. Mater.* **1998**, *1*, 286–294. [CrossRef]
13. Shin, D.H.; Kim, H.J. Influence of the lateral restoring force of isolation system to the seismic performance of isolated buildings in low-to-moderate seismicity regions. *Soil Dyn. Earthq. Eng.* **2019**, *125*, 105706. [CrossRef]
14. ASCE. *Minimum Design Loads for Buildings and Other Structures: ASCE/SEI 7*; American Society of Civil Engineers: Reston, VA, USA, 2016.
15. AIK. *Korean Building Code: KBC2016*; Architectural Institute of Korea: Seoul, Korea, 2016.
16. Krawinkler, H.; Zaraian, F.; Lignos, D.G.; Ibarra, L.F. Significance of modelling deterioration in structural components for predicting the collapse potential of structures under earthquake excitations. In *Advances in Performance-Based Earthquake Engineering. Geotechnical, Geological and Earthquake Engineering*; Springer: Dordrecht, The Netherlands, 2010.
17. FEMA. *Quantification of Building Seismic Performance Factors: FEMA P695*; Federal Emergency Management Agency: Washington, DC, USA, 2009.

18. Parsaeimaram, M.; Fang, C.; Luo, X.; Shaya, C. Seismic performance evaluation of double-skin semi-base-isolated building using incremental dynamic analysis. *Adv. Civ. Eng.* **2018**, *2018*, 2747836. [CrossRef]
19. Nakazawa, N.; Kishiki, S.; Qu, Z.; Miyoshi, A.; Wada, A. Fundamental study on probabilistic evaluation of the ultimate state of base isolated structures. In Proceedings of the 8CUEE Conference Proceedings, 8th International Conference on Urban Earthquake Engineering, Tokyo, Japan, 7–8 March 2011.
20. Erduran, E.; Dao, N.D.; Ryan, K.L. Comparative response assessment of minimally compliant low-rise conventional and base-isolated steel frames. *Earthq. Eng Struct Dynam.* **2011**, *40*, 1123–1141. [CrossRef]
21. Sayani, P.J.; Erduran, E.; Ryan, K.L. Comparative response assessment of minimally compliant low-rise base-isolated and conventional steel moment-resisting frame buildings. *J. Struct. Eng.* **2011**, *137*, 1118–1131. [CrossRef]
22. Terzic, V.; Mahin, S.A.; Comerio, M.C. Comparative Life-cycle cost and performance analysis of structural systems for buildings. In Proceedings of the 10th National Conference in Earthquake Engineering, Anchorage, AK, USA; 2012.
23. McVitty, W.J.; Constantinou, M.C. *Property Modification Factors for Seismic Isolators: Design Guidance for Buildings*; Multidisciplinary Center for Earthquake Engineering Research: Buffalo, NY, USA, 2015.
24. Kitayama, S.; Constantinou, M.C. Collapse performance of seismically isolated buildings designed by the procedures of ASCE/SEI 7. *Eng. Struct.* **2018**, *164*, 243–258. [CrossRef]
25. Christopoulos, C.; Filiatrault, A. *Principles of Passive Supplemental Damping and Seismic Isolation*; IUSS Press: Pavia, Italy, 2006.
26. Pant, D.R.; Wijeyewickrema, A.C. Performance of base-isolated reinforced concrete buildings under bidirectional seismic excitation considering pounding with retaining walls including friction effects. *Earthq. Eng. Struct. Dyn.* **2014**, *43*, 1521–1541. [CrossRef]
27. Masroor, A.; Mosqueda, G. Assessing the collapse probability of base-isolated buildings considering pounding to moat walls using the FEMA P695 methodology. *Earthq. Spectra.* **2015**, *31*, 2069–2086. [CrossRef]
28. Computers and Structures Inc. *PERFORM Components and Elements for Perform 3D and Perform-Collapse Ver 4*; Computers and Structures, Inc.: Berkerley, CA, USA, 2006.
29. FEMA. *Prestandard and Commentary for the Seismic Rehabilitation of Buildings*; Federal Emergency Management Agency: Washington, DC, USA, 2000.
30. FEMA. *HAZUS-MH, MH2.0 Earthquake Model Technical Manual*; Federal Emergency Management Agency: Washington, DC, USA, 2003.
31. Zhang, J.; Huo, Y. Evaluating effectiveness and optimum design of isolation devices for highway bridges using the fragility function method. *Eng. Struct.* **2009**, *31*, 1648–1660. [CrossRef]
32. Han, R.; Li, Y.; Lindt, J. Seismic risk of base isolated non-ductile reinforced concrete buildings considering uncertainties and mainshock-aftershock sequences. *Struct. Saf.* **2014**, *50*, 39–56. [CrossRef]
33. Vamvatsikos, D.; Fragiadakis, M. Incremental dynamic analysis for estimating seismic performance sensitivity and uncertainty. *Earthq. Eng. Struct. Dyn.* **2009**, *39*, 141–163. [CrossRef]
34. Shin, D.H.; Yang, W.J.; Kim, H.J. Comparative Evaluation of Probabilistic Uncertainty-Propagations to Seismic Collapse Capacity of Low-Rise Steel Moment-Resisting Frames. *Int. J. Steel Struct.* **2016**, *16*, 887–900. [CrossRef]
35. Ellingwood, B. *Reliability Basis of Load and Resistance Factor for Reinforced Concrete Design: National Bureau of Standards Buildings Science Series 110*; National Bureau of Standards: Washington, DC, USA, 1978.
36. Celik, O.C.; Ellingwood, B. Seismic fragilities for non-ductile reinforced concrete frames-Role of aleatoric and epistemic uncertainties. *Struct. Saf.* **2010**, *32*, 1–12. [CrossRef]
37. Porter, K.A.; Beck, J.L.; Shaikhutdinov, R.V. Sensitivity of building loss estimates to major uncertain variables. *Earthq. Spectra.* **2002**, *18*, 719–743. [CrossRef]
38. Baker, J.W. Vector-Valued Ground Motion Intensity Measures for Probabilistic Seismic Demand Analysis. Ph.D. Thesis, Department of Civil and Environmental Engineering, Stanford University, Stanford, CA, USA, 2005.
39. Baker, J.W.; Cornell, C.A. Spectral shape, epsilon and record selection. *Earthq. Eng. Struct. Dyn.* **2006**, *35*, 1077–1095. [CrossRef]
40. Haselton, C.B.; Baker, J.W.; Liel, A.B.; Deierlein, G.G. Accounting for ground-motion spectral shape characteristics in structural collapse assessment through an adjustment for Epsilon. *J. Struct. Eng.* **2011**, *137*, 332–344. [CrossRef]

41. Abrahamson, N.A.; Silva, W.J. Empirical response spectral attenuation relations for shallow crustal earthquakes. *Seismol. Res. Lett.* **1997**, *68*, 94–127. [CrossRef]
42. Shin, D.H.; Hong, S.J.; Kim, H.J. Investigation on Effective peak ground accelerations based on the Gyeongju Earthquake records. *Eesk. J. Earthq. Eng.* **2016**, *20*, 425–434. [CrossRef]
43. United States Geological Survey. Earthquake Hazards Program-Unified Hazard Tool. Available online: https://earthquake.usgs.gov/hazards/interactive/ (accessed on 16 April 2020).